

Protoplanetary disk chemistry and structure

Merel L.R. van 't Hoff^{a,b} and Jennifer B. Bergner^c

^aUniversity of Michigan, Department of Astronomy, 1085 S. University Ave., Ann Arbor, MI 48109-1107, USA

^bPurdue University, Department of Physics and Astronomy, 525 Northwestern Avenue, West Lafayette, IN 47907, USA

^cUniversity of California, Berkeley, Department of Chemistry, Berkeley, CA 94720, USA

© 20xx Elsevier Ltd. All rights reserved.

Abstract

Knowledge of the composition of material that will form planets is crucial to understand planetary diversity and the occurrence of potentially habitable planets. Ultimately, it is the chemistry in circumstellar disks that determines the global make up of planetary systems, as the dust in these disks grows into giant planet cores and rocky planets, the gas becomes incorporated in giant planet atmospheres, and the ices can be delivered to rocky planets by comets and meteorites. With the advent of ALMA a decade ago and the recent launch of JWST, the composition of the disk gas and ice can now be studied in great detail. This review will provide an overview of our current knowledge of the disk chemical structure, focusing on the six elements essential to life on Earth: carbon (C), hydrogen (H), nitrogen (N), oxygen (O), phosphorus (P) and sulfur (S).

Keywords

Astrochemistry, circumstellar disks, circumstellar gas, circumstellar dust, molecular gas, ice composition, small molecules, millimeter astronomy, submillimeter astronomy, infrared astronomy.

Glossary

Chemical inheritance Molecules formed during a certain stage of star formation become incorporated unaltered into the next stage.

Chemical reset Molecules formed during a certain stage of star formation are destroyed or altered before becoming incorporated into the next stage. Also referred to as 'processing'.

CHNOPS The six elements essential to life on Earth: carbon (C), hydrogen (H), nitrogen (N), oxygen (O), phosphorus (P) and sulfur (S).

Coma Cloud of gas and dust produced from a comet's surface, caused by ice sublimation when the comet passes close to the sun.

Complex organic molecule In the context of astrochemistry, a carbon-bearing molecule containing at least six atoms.

Condensation Phase change from gas to ice. Often referred to as 'freeze out' or 'depletion'.

Depletion Generally, the removal of a molecular species from a certain phase, and is often used to describe the phase change from gas to ice (also referred to as 'freeze out' or 'condensation'). It is also more loosely used to indicate a lower molecular abundance in the gas beyond the 'loss' expected from ice formation alone.

Desorption Phase change from ice to gas. Also referred to as 'sublimation'.

Deuterium Heavy isotope of hydrogen containing a proton and a neutron in the nucleus.

Dissociation Destruction of the bond between two atoms.

Endothermic reaction Reaction that consumes energy.

Envelope Remnant of the parent molecular cloud that shrouds a newly forming star. Infall of the envelope results in accretion of material onto the disk and protostar.

Exothermic reaction Reaction that releases energy.

Freeze out Phase change from gas to ice. Also referred to as 'condensation' or 'depletion'.

Freeze-out temperature Temperature at which a molecular species transitions from being primarily present in the gas phase to being primarily present in the ice. Often interchangeably used with 'sublimation temperature'.

Habitable A planet that is potentially hospitable to life. Generally implies a rocky/terrestrial planet composition with a temperate climate allowing for the existence of liquid water, and access to biogenic elements (CHNOPS).

Herbig star A young star on the high end of the stellar mass spectrum, more than two times as massive as the sun.

Hydrogenation The addition of an hydrogen (H) atom to a molecule.

Ice line Radius in the disk midplane where the temperature is equal to the freeze-out temperature of a molecular species. Inside its ice line, a molecular species is predominantly present in the gas phase, while outside its ice line it is predominantly present in the ice. Also referred to as 'snowline'.

Interferometer Array of correlated telescope antennae which are combined to produce images with high spatial resolution.

Ion Atom or molecule with a net electrical charge due to the addition or removal of electrons, causing the positive charge of the nucleus and negative charge of the electrons to no longer balance out. Most ions in disks are positively charged.

Ionization Process converting electrically neutral atoms or molecules into charged atoms or molecules (ions) through the addition or removal of electrons. In disk environments, electron removal is the dominant ionization process.

2 Protoplanetary disk chemistry and structure

Isotopes Different ‘versions’ of an element due to different numbers of neutrons in their nuclei (e.g., ^{12}C and ^{13}C).

Isotope fractionation Preferential enrichment or depletion of a particular isotope in a molecular reservoir relative to the cosmic isotope ratio.

Isotopologues Different ‘versions’ of a molecular species due to incorporation of different isotopes (e.g., $^{12}\text{C}^{16}\text{O}$, $^{13}\text{C}^{16}\text{O}$ and $^{12}\text{C}^{18}\text{O}$).

Line emission/absorption Discrete spectral feature due to a transition between two quantum states of an atom or molecule that involves the emission or absorption of a photon.

M dwarf The lowest-mass class of stars (less than roughly half the mass of the sun). M dwarfs are the most common type of star.

Midplane Equatorial plane of the protoplanetary disk, characterized by the coldest and densest conditions. Planet formation takes place within the midplane.

Molecular layer Chemically rich vertical layer in the disk that is sufficiently shielded from UV radiation to not destroy all molecules and warm enough to prevent molecules from being present only as ice.

Photoablation The removal of atoms and/or small molecules from grain surfaces by energetic photons.

Photodesorption Phase change from ice to gas induced by UV or X-ray photons.

Photodissociation Destruction of the bond between two atoms upon absorption of a UV or X-ray photon.

Radical Atom, molecule, or ion that has at least one unpaired electron.

Refractory material Material that remains solid up to high temperature (a few 100 to a few 1000 Kelvin, depending on the composition of the material). Typically referred to as ‘dust grains’.

Self-shielding Ability of certain molecular species (e.g., H_2 , CO , N_2 , H_2O) to protect themselves from photodissociation as these molecules dissociate only upon absorbing photons of specific wavelengths. If a large enough column of these molecules is present, molecules in the top layer absorb all dissociating photons, protecting molecules at deeper layers.

Snowline Radius in the disk midplane where the temperature is equal to the freeze-out temperature of a molecular species. Inside its snowline, a molecular species is predominantly present in the gas phase, while outside its snowline it is predominantly present in the ice. Also referred to as ‘ice line’.

Snow surface Vertical height in the disk, varying with radius, where the temperature is equal to the freeze-out temperature of a molecular species. Above its snow surface, a molecular species is predominantly present in the gas phase, while below its snow surface it is predominantly present in the ice.

Solids Material in either refractory (dust grains) or ice form.

Speciation The distribution of an element amongst chemical species.

Sublimation Phase change from ice to gas. Often referred to as ‘desorption’.

Sublimation temperature Temperature at which a molecular species transitions from being primarily present in the ice to being primarily present in the gas. Often interchangeably used with ‘freeze-out temperature’.

T Tauri star A young star on the low end of the stellar mass spectrum, less than two times the mass of the sun.

Volatility Tendency for a molecule to exist in the gas versus solid state, related to its binding energy. Generally treated as a spectrum from hypervolatiles (e.g. CO , N_2 , CH_4) to volatiles (CO_2 , H_2O , CH_3OH) to (semi-)refractories (NH_4^+ salts, amorphous/mineral solids).

Nomenclature

ALMA	Atacama Large Millimeter/submillimeter Array
CHNOPS	Carbon, Hydrogen, Nitrogen, Oxygen, Phosphorus, Sulfur
IR	Infrared
ISM	Interstellar medium
JWST	James Webb Space Telescope
LTE	Local Thermodynamic Equilibrium
PDR	Photodissociation region
UV	Ultraviolet

Learning objectives

By the end of this chapter you will understand

- What can be learned from molecular line observations
- How molecules in disks can be observed
- The main processes important for the chemistry in disks
- The global chemical structure of disks
- What the main carriers are for the six elements essential to life on Earth
- What snowlines are and their relevance to planet formation

1 Introduction: why study disk chemistry?

With the detection of several thousand planets around stars other than our Sun in the last decades and the capability of JWST and (upcoming) ground-based facilities to study their atmospheres in great detail, we are entering an exciting era of characterizing planets and searching for Earth-like and potentially habitable planets. Constraining the origin of different types of planets and how common or rare they may be requires a detailed understanding of the chemical composition of the gas and solids from which planets form (Fig. 1). For example, in the simplest view, which molecules are present in the gas at the formation location of a giant planet will determine the elemental composition of its atmosphere. In addition, the condensation ('freeze-out') of molecules onto dust grains may influence the growth of small grains into larger bodies, directly impacting the planet formation process itself. Furthermore, emission from molecules probes the physical conditions, such as temperature and ionization level, that are important to understand disk evolution and planet formation. Finally, molecular emission reveals the kinematics in the disk, providing a way to infer the presence of forming planets. Chemistry in protoplanetary disks has therefore been a topic of many observational and modeling studies. This review aims to summarize the current state of the field at a level suitable to non-experts and early-career scientists.

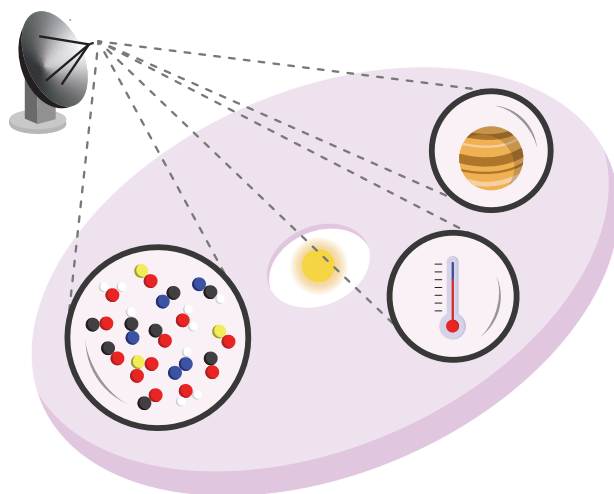


Fig. 1 Cartoon illustrating an example of different aspects of protoplanetary disks that can be studied with molecular line observations: the chemical content of the gas and ice that may be incorporated into planets, physical properties such as temperature, and disturbances in the disk velocity structure due to forming planets.

We will here focus on the six elements essential to life on Earth: carbon (C), hydrogen (H), nitrogen (N), oxygen (O), phosphorus (P) and sulfur (S)– often abbreviated as CHNOPS. In the interstellar medium (ISM), these elements can exist either in a refractory form (solid phase unless the temperature exceeds a few hundred Kelvin, referred to as dust grains) or a volatile form (either gas or ice depending on the temperature) (Fig. 2). The speciation of these elements into different chemical carriers within a protoplanetary disk profoundly impacts the outcomes of planet formation, and will be discussed in detail in this review. We will focus on the volatile states (gas and ice), as those can be probed directly with infrared and (sub)millimeter observations.

It is important to recognize that the chemical makeup of a protoplanetary disk is, to some degree, influenced by the chemistry of earlier evolutionary stages. The process of star and planet formation begins with a dense molecular cloud in which about half of the total available carbon, a substantial fraction of oxygen, and the majority of sulfur and phosphorus are present in refractory dust grains. Despite the relatively low densities (10^4 – 10^5 particles cm^{-3}) and low temperatures (~ 10 K), that make it hard for two atoms to find each other and react, molecules do form from the remaining volatile atoms. H_2 and CO are the most abundant molecules in the molecular cloud gas, but most material is frozen in an icy layer on the surface of the dust grains. Ice mantles are host to a rich chemistry leading to the production of simple hydrides (e.g. H_2O , CH_4 , NH_3), as well as CO_2 and so-called ‘complex’ organic molecules: C-bearing molecules containing at least six atoms. During collapse of the molecular cloud to form a protostar, the ice and gas are subjected to heating and radiation processing, which leads to further chemical processing and increases the degree of chemical complexity present in both the gas and ice phase. This protostellar material represents the initial chemical conditions for a protoplanetary disk. The chemical state of a disk is likely a combination of inherited cloud/protostellar material, and material that undergoes further processing in the unique disk physical environment. The balance between chemical inheritance and reprocessing, as well as the coupling between physics, dynamics, and chemistry, are both major themes in the study of protoplanetary disk chemistry.

This chapter is structured as follows. Section 2 starts with a brief overview of the disk physical structure, focusing on aspects directly impacting the chemistry. Section 3 then introduces the dominant processes for gas-phase (Sect. 3.1) and ice-phase (Sect. 3.2) chemistry. The resulting disk chemical structure in vertical (Sect. 4.1) and radial (Sect. 4.2) directions is detailed in Sect. 4. Differences between

4 Protoplanetary disk chemistry and structure

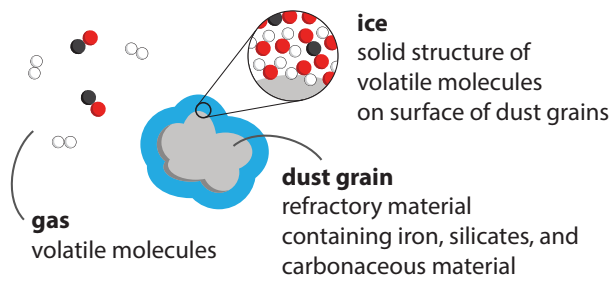


Fig. 2 Illustration of the three forms, or phases, atoms and molecules can take in disks. Refractory elements such as iron (Fe), magnesium (Mg) and silicon (Si) are almost exclusively present in dust grains (unless the temperature exceeds hundreds of Kelvin). These refractory grains also contain significant amounts of carbon (C) and oxygen (O). More volatile elements (CHNOPS) are either present as gas or ice on the surface of the dust grains, depending on the temperature (see Section 4.2).

young and mature disks are briefly described in Sect. 4.3. A description of the main CHNOPS carriers in disks is given in Sect. 5, and the chemistry for their isotopes is presented in Sect. 6. Sections 7 and 8, respectively, detail our knowledge about (complex) organic molecules in disks and chemical substructures. Finally, a brief introduction to molecular line observations and spectroscopy at microwave (Sect. 9.1) and infrared (Sect. 9.2) wavelengths is presented in Sect. 9, and a succinct overview of analysis techniques and models is given in Sect. 10. We end with a brief outlook for the future (Sect. 11).

2 Protoplanetary disk physical structure

Protoplanetary disks are host to a wide range of physical conditions, spanning cold quiescent environments similar to a molecular cloud, to hot irradiated environments similar to a photodissociation region (PDR). Overall, there are strong vertical and radial gradients in the physical structure. The density increases moving from the disk surface to the midplane in the vertical direction, and decreases moving from the star towards the outer disk in the radial direction. The temperature and radiation fields decrease from the disk surface to the midplane, and decrease from the inner to outer disk. A schematic of the physical structure is presented in Fig. 3, and a more detailed discussion is presented by e.g., Henning and Semenov (2013).

Temperature

The thermal structure of the disk is determined by the processing of stellar and interstellar radiation by dust particles. The main heating mechanism in the disk surface is called photoelectric heating, which proceeds as follows. When a UV (ultraviolet) photon hits a dust grain, part of its energy can free an electron from the grain surface, while the remaining energy heats the grain itself. The free electrons in turn interact with and heat the gas. In the region of the disk closest to the star, accretion heating (loss of gravitational energy as gas accretes onto the star) can also play a dominant role in heating the dust grains. As the accretion rate typically decreases with age, this process is expected to be most important in young disks that are still embedded in remnants of the parent cloud. Dust grains in the bulk of the disk are heated by infrared radiation from other grains. This way, heating of grains in the inner region and surface layers of the disk results in a cascade of absorption and re-emission of infrared radiation by dust grains throughout the disk. The gas, in turn, is heated through collisions with the dust. The main cooling mechanism for the disk is the emission of thermal radiation from the dust grains, which peaks in the infrared. In most of the disk, the density is high enough for collisions between gas and dust to be frequent enough that the gas temperature is equal to the dust temperature. This is not the case in the upper surface layers, where the gas and dust temperature are decoupled, and the gas temperature is determined by the balance of photoelectric heating versus cooling through atomic and molecular line emission.

Density

The radial surface-density (density integrated over the full height of the disk) profile of disks can be approximated on large spatial scales by a power-law with an exponential fall off towards the outer edge. It is typically assumed that the dust surface density is 100× smaller than the gas surface density based on interstellar gas-to-dust ratios, though it is contested whether the same ratio should hold in disks. Recently, high-resolution observations with ALMA have revealed that the small-scale dust distribution is not, in most cases, well described by a smoothly varying power-law surface density profile: the dust is often locally concentrated in rings or spiral structures, referred to as dust ‘sub-structures’. Similarly, high-resolution observations have shown that disk gas molecules exhibit sub-structuring. It remains unclear to which extent the bulk gas (H₂) is substructured or whether this is a chemical effect (see more in Section 8). The millimeter dust is generally more radially compact than the gas due to drift of large solids towards the star, though it is difficult to measure disk sizes precisely because of the vanishing emission at the cold and low-density outer edge. The vertical distribution of gas in disks is often considered to be set by hydrostatic equilibrium, where gravity and thermal pressure are in equilibrium, and the ratio of thermal to gravitational energy increases with disk radius. While the small dust should remain well coupled to the gas, larger dust grains will ‘settle’ to a more vertically compact region near the midplane. In outer disk regions, gravity becomes too weak to confine the material to a thin plane and the thermal energy expands the disk in the vertical direction. This puffing up of the outer disk is called ‘flaring’.

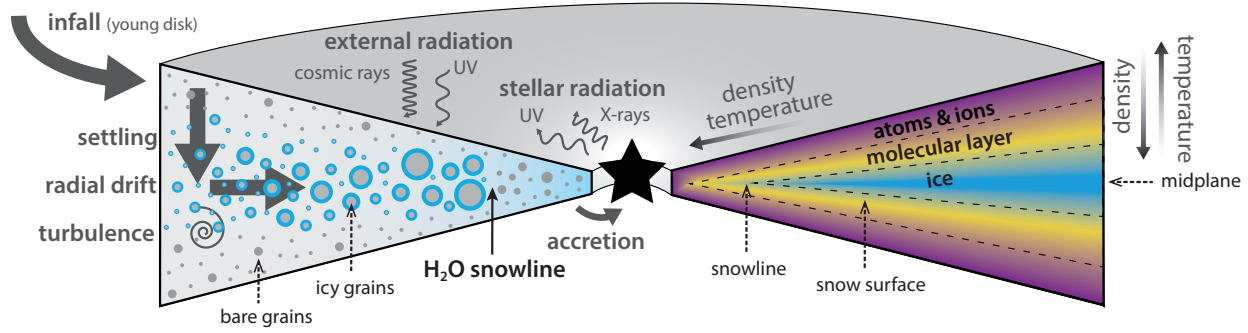


Fig. 3 Illustration of the physical and chemical structure of protoplanetary disks. Young embedded disks, also called protostellar disks, are expected to have a similar structure albeit warmer with less dust evolution (i.e., settling, drift and growth) and are embedded in remnants of the parent cloud, called the envelope. Infall of material on the disk is therefore most important for young disks.

Radiation

In addition to heating the disk, the radiation field also plays a direct role in the chemistry, inducing processes like ionization and dissociation which drive subsequent reactions (Section 3). Of particular importance are UV radiation, X-rays and cosmic rays. UV radiation is generated by the accretion shock from material falling onto the star and in the stellar photosphere. This type of radiation has the smallest penetration depth and is only present in the surface layers of the disk. Small dust grains are the major source of UV opacity, and so the UV field is strongly dependent on the dust distribution. X-ray emission can penetrate deeper into the disk and young stars show strong X-ray emission due to their enhanced stellar and magnetic activity compared to more evolved stars. Cosmic rays have the largest penetration depth and can provide a source of ionization in the disk midplane. The amount of cosmic rays present in disks is still uncertain: on the one hand stellar winds may reduce the flux of galactic cosmic ray particles impinging onto the disk. On the other hand, cosmic rays may be created locally through the acceleration of particles at shock surfaces (see e.g., the discussion by Zhang 2024).

Dust dynamics

As already hinted at, dynamics plays an important role in setting the physical structure of a disk. In the vertical direction, large grains tend to gravitationally settle towards the midplane, while turbulence can stir material from the midplane back to the surface layers. In the radial direction, a phenomenon called ‘radial drift’ acts on intermediate-sized dust grains (often called ‘pebbles’): as the gas orbits at sub-Keplerian velocities due to gas pressure support, intermediate-size grains experience a headwind. Due to this gas drag, they lose angular momentum and spiral towards the region of maximum pressure. In a smooth disk this means that pebbles drift into the star, though the presence of local pressure maxima (pressure ‘bumps’) can halt the drift of pebbles at disk substructures. Smaller grains are well coupled to the gas and do not experience radial drift. Larger solids follow Keplerian orbits and are not meaningfully influenced by the presence of the slower-moving gas. The exact grain size that is susceptible to gas drag depends on many factors and varies as a function of disk radius, but is typically around millimeter–centimeter scale. The ongoing growth and fragmentation of grains throughout the disk lifetime means that settling, turbulence, and drift are operating on a constantly evolving population of dust grains. These dynamical processes are greatly important to disk chemistry, since they impact the physical conditions (radiation field, temperature, ionization) and also result in transport of volatiles between different disk regions. Lastly, the disk physical conditions can also evolve due to the astrophysical context of star formation: for example, disks are expected to cool as accretion onto the star slows down and the envelope dissipates, while short periods of enhanced accretion (so-called ‘accretion bursts’) result in temporary increases in temperature.

3 Astrochemical processes

Throughout much of the disk, the temperatures and densities are too low for the gas chemistry to reach steady-state, that is, a state in which the molecular abundances are set by the current physical conditions and do not change over time (as long as the physical conditions do not change). Instead, molecular abundances depend on the relative rates of different chemical reactions and change during the lifetime of the disk, even if the physical conditions remain constant. As reaction rates depend on physical conditions, the molecular abundances at any time depend on the physical conditions at current and past times. Infrared surveys of large populations of disks suggest a median dust-disk lifetime of several million years, indicating that chemical processes must operate on shorter timescales to be relevant in disks, although the lifetime of the gas disk is more uncertain. Reaction pathways and rates are typically derived from laboratory experiments or quantum-physical calculations. Reactions can take place either in the gas phase or within the icy mantles coating grain surfaces (Fig. 4). Some molecules have formation pathways both in gas and ice phases (e.g. formaldehyde, H_2CO), while other molecules are thought to form in only one phase (e.g., methanol, CH_3OH , can only form on a grain surface).

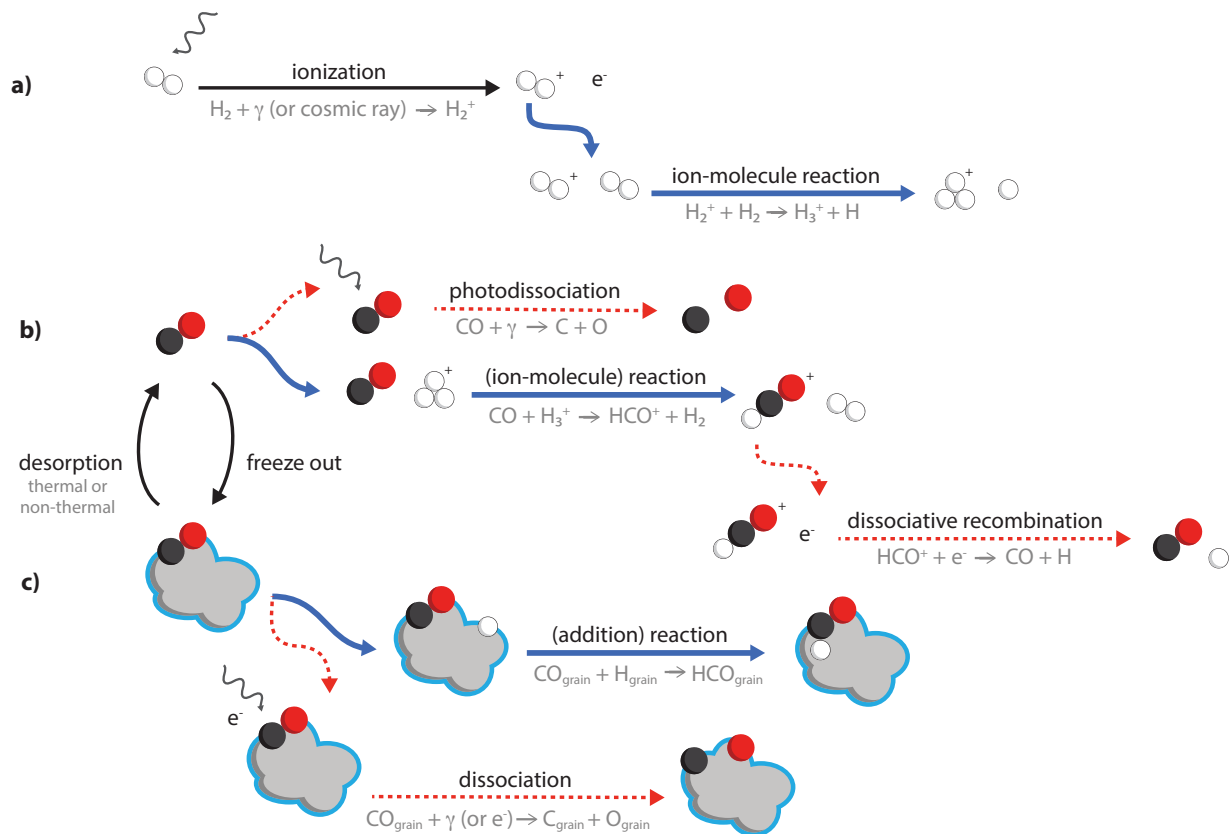


Fig. 4 Illustration of the main chemical reaction types in disks. The dominant ionization pathway (a) results in the formation of the H_3^+ ion. Examples of different types of gas-phase (b) and ice-phase reactions (c) are shown for CO, but also apply to other molecules. Routes that lead to the formation of new molecules and potentially greater chemical complexity are shown in blue, and destruction routes are shown in red. Photons are denoted with γ in the reactions.

3.1 Gas-phase chemistry

3.1.1 Bulk of the disk

At the low temperatures (< 100 K) present in the bulk of the disk, reactions may proceed only if they (i) release energy ('exothermic' reactions) and (ii) do not have an activation energy barrier. At the same time, the low-to-intermediate densities ($\lesssim 10^8 \text{ cm}^{-3}$) favor so-called two-body reactions which do not require a third colliding species to dissipate reaction energy. Reactions between two neutral molecules are typically endothermic and/or have an activation barrier, whereas the transfer of a proton from an ion to a neutral molecule is usually exothermic and barrierless. Ion-neutral chemistry therefore dominates in the bulk of the disk gas.

Ion-neutral reactions

To drive ion-neutral reactions, and thus gas-phase chemistry, a source of ionization (UV radiation, X-rays, cosmic rays or radionuclides) is needed. An ionization event typically leads to H_3^+ formation since hydrogen is the most abundant element. H_3^+ then powers a rapid ion-molecule chemistry which can lead to the production of complex molecular ions (Fig. 4). For example, H_3^+ can transfer a proton to CH_2 to form CH_3^+ . This molecular ion can then react with HCN, forming CH_3CNH^+ .

Dissociative recombination reactions

Neutral molecules can be formed through a process called dissociative recombination, in which a free electron recombines with a molecular ion which then dissociates into two stable molecules or a molecule and atom. This can produce both simple and relatively large neutral molecules. For example, CH_3CNH^+ can recombine with an electron to form CH_3CN and a hydrogen atom.

Other reaction types

In addition to driving the formation of molecules, radiation also leads to their destruction, as molecular bonds can be broken upon absorption of UV photons in a process called photodissociation. While other gas-phase molecule formation pathways, such as neutral-neutral reactions (reaction between two neutral molecules, producing two different neutral species) and radiative association (reaction between two atoms or

molecules forming a larger molecule while emitting a photon), are possible, they are in most cases much less efficient than ion-molecule chemistry.

3.1.2 Inner disk

At the high temperatures ($\sim 100 - 5000$ K) and densities ($\gtrsim 10^{12} \text{ cm}^{-3}$) in the inner few au of the disk, the chemistry is fast enough to approach equilibrium. Even so, dynamical processes may prevent equilibrium from being reached. In the absence of intense sources of ionizing radiation, neutral-neutral reactions with barriers $\gtrsim 100 - 1000$ K start playing an important role, and 3-body reactions become important in regions with densities $> 10^{12} \text{ cm}^{-3}$. Molecules remain abundant in the gas phase until the temperature exceeds $\sim 2500 - 3500$ K at the inner edge of the disk, where they are destroyed by thermal dissociation.

3.2 Ice chemistry

3.2.1 Transitions between gas and ice

A major factor governing the chemical structure of disks is the partitioning of molecules between the gas phase and the frozen/solid phase, called the ‘ice’ phase. A given molecule’s tendency to exist in the gas or solid phase, referred to as its ‘volatility’, is determined by its binding energy: the strength of interaction between the molecule and a solid surface. In the case of interstellar ice molecules, the surface is typically an amorphous H_2O -dominated ice layer (that is, the molecules are arranged in a disordered rather than crystalline state) which coats a refractory dust grain. A ‘freeze-out temperature’ is often used to approximate the temperature at which a molecule transitions from primarily gas-phase to primarily ice-phase (though this balance formally depends on the density as well). Molecules with lower binding energies have lower freeze-out temperatures, i.e. remain in the gas phase down to lower temperatures. ‘Freeze-out’ and ‘condensation’ are usually used synonymously to describe the removal of gas-phase molecules onto dust grains. The term ‘depletion’ is also used sometimes, but this is not recommended due to the more ambiguous meaning. Similarly, ‘sublimation’ and ‘desorption’ both describe the ice to gas transition.

Ice-phase molecules can be desorbed into the gas phase either by thermal desorption, if the grain is warmer than the molecule’s sublimation temperature, or via non-thermal desorption mechanisms. Photodesorption refers to desorption induced by photons like UV or X-rays, and cosmic rays can also cause ice desorption. Typically, only small molecules can be photodesorbed intact, whereas larger molecules are photodesorbed as fragments. Excess energy released upon the formation of a molecule on the grain surface may also result in its sublimation, called chemical desorption or reactive desorption.

3.2.2 Reactions in the ice

Molecules can still participate in active chemistry after freezing out onto grains (Fig. 4). In fact, ice-phase chemistry is more efficient than gas phase chemistry for certain reaction classes, including the formation of many organic molecules. Importantly, the ice mantle can dissipate excess reaction energy (acting as a ‘third body’), stabilizing products which would otherwise dissociate into fragments in the gas phase. This explains why some molecules like H_2 and CH_3OH cannot form in the gas phase, but can form on grain surfaces. Ices also concentrate potential reactants and enable multiple reaction attempts for barriered reactions.

New molecules can form in the ice through either ‘energetic’ or ‘non-energetic’ pathways. Energetic processing refers to chemical processes induced by photons, electrons, or cosmic rays, which dissociate stable molecules into highly reactive radical species (atom or molecule with at least one unpaired electron). These radicals can recombine barrierlessly with neighboring radicals to form larger molecules, or if the grain temperature is high enough, radicals can diffuse over the surface to encounter new reaction partners. Non-energetic chemistry is driven by atom addition and abstraction reactions, in which atomic species (mainly H, but also potentially O) are added to or removed from a stable molecule. In both cases, the result is the formation of reactive radical species that can, once again, recombine with other radicals to form larger molecules. While most neutral-neutral reactions cannot be thermally activated at temperatures relevant to ices (≤ 150 K), a notable exception is the formation of ammonium salts, which can occur at a few tens of K.

4 Protoplanetary disk chemical structure

4.1 Vertical structure

The strong temperature and density gradients together with differences in the radiation fields at various disk locations create a three-layered chemical structure in the vertical direction (Fig. 3; (Aikawa and Herbst, 1999)).

The surface layer

In the disk surface layers, the chemistry is dominated by photoprocesses. The stellar UV radiation and the interstellar radiation field ionize and dissociate molecules. The disk surface therefore has parallels with regions in the dense interstellar medium that are irradiated by massive stars, so-called photodissociation regions (PDRs). Molecules that are dissociated by line radiation (i.e., dissociated by light at specific frequencies), for example, H_2 , CO and N_2 , can self-shield at sufficiently high column densities. This means that all radiation at the specific dissociative frequencies gets absorbed by molecules closest to the disk surface, protecting molecules deeper in the disk (Fig. 5). In addition, as photons with certain frequencies can dissociate both H_2 and CO (or H_2 and N_2), H_2 can partially shield CO and N_2 . Water (H_2O) is another molecule present in the disk surface layer because, in addition to self-shielding, it can form efficiently via neutral-neutral

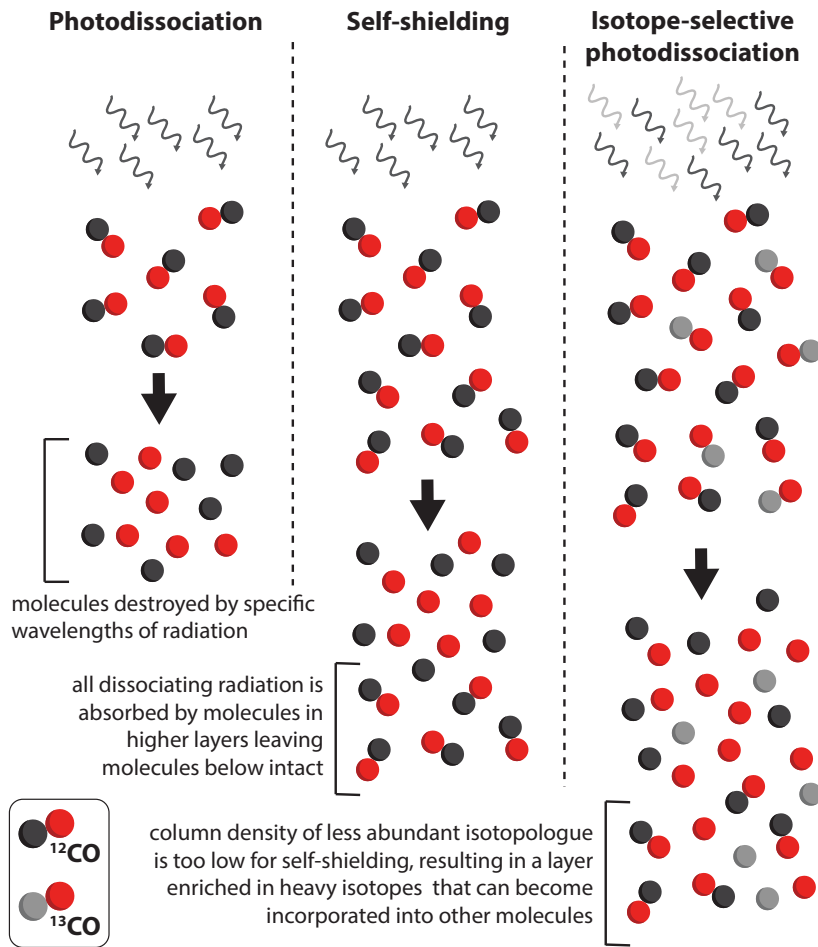


Fig. 5 Illustration of photodissociation by line emission (left), where molecules are destroyed by radiation of specific wavelengths, self-shielding (middle), where the top layer of molecules absorbs all dissociating radiation protecting the molecules in deeper layers, and isotope-selective photodissociation (right), where the less abundant isotopologue has a column density too low for self-shielding, resulting in a layer enriched in the rare isotope that can then become incorporated into other molecules.

reactions when the gas temperature is higher than 400 K. X-ray photons can penetrate deeper into the disk than UV photons and ionize helium, producing He^+ which is able to destroy tightly bound molecules like CO, therefore driving a rapid hydrocarbon chemistry.

The warm molecular layer

Underneath the disk surface is a warm molecular layer that is sufficiently shielded from UV irradiation such that not all molecules are destroyed. The survival of molecules leads to a rich chemistry that is driven by X-rays. As the temperature in this layer is $\sim 30\text{--}70$ K, the least volatile molecules such as H_2O and NH_3 will be frozen onto the dust grains. The freeze-out of water, and consequently the removal of a large fraction of the oxygen budget from the gas phase, results in carbon-to-oxygen (C/O) ratios elevated above the disk overall value, leading to a carbon-dominated gas chemistry (more in Sect. 5.2). Furthermore, these lukewarm temperatures allow for grain surface chemistry resulting in, for example, formation of formaldehyde (H_2CO). In less opaque regions (e.g., in the outer disk), UV photons may drive photodesorption of ice species. As the UV opacity is dominated by small dust grains, grain growth and settling allows ionizing and dissociating photons to penetrate deeper into the disk. The vertical extent of the warm molecular layer is thus strongly coupled to the evolution of the dust.

The midplane

The deep interior of the disk is completely shielded from UV and X-ray radiation, causing the temperature to drop below 20 K. Freeze-out of molecules and hydrogenation reactions on grain surfaces dominate the chemistry. Because of its low binding energy to grain surfaces, H_2 will remain in the gas even in the midplane, but most other molecules are expected to be frozen out. Ice-phase chemistry may still proceed in the midplane to some extent if cosmic rays are present, though it is generally thought to be rather chemically inactive.

Most of the molecular line emission from disks thus originates from the chemically-rich warm molecular layer or near the disk midplane inside that molecule's snowline. The exact emitting region for a molecular transition will depend on the chemistry that determines where a molecule is most abundant, and on excitation, as higher-energy transitions will be excited in warmer gas than lower-energy transitions. In edge-on disks, vertical stratification of different molecules and transitions can be observed directly, while for more face-on disks the emitting height of molecular emission can be inferred from observations with high spatial and spectral resolution (Fig. 6).

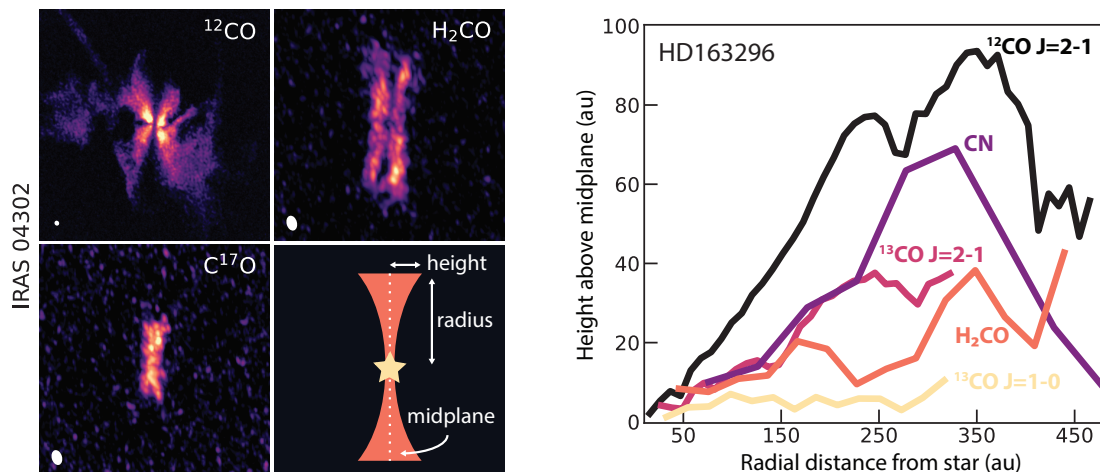


Fig. 6 Examples of vertical stratification in disks. The vertical structure can be probed directly in edge-on disks, as shown for the young disk IRAS 04302 (left; ALMA observations originally presented by van 't Hoff et al. 2020 and Lin et al. 2023). In less inclined disks such as HD163296, the emitting height can be derived from observations with high spectral and spatial resolution (right; adapted from Paneque-Carreño et al. 2023; ©ESO).

4.2 Radial structure and snowlines

In the disk midplane, molecules will freeze onto dust grains when the temperature drops below a given molecule's freeze-out temperature. The midplane radius where this happens is referred to as the radial 'snowline' or 'ice line'. Each molecule has a unique snowline location determined by its freeze-out temperature. Combined with the radial temperature gradient in the disk, this results in sequential freeze out of different molecules, with the least volatile molecules freezing out closest to the star (Fig. 7). For example, the H_2O snowline is located at temperatures of ~ 150 K, corresponding to a few au for T Tauri stars, while CO does not freeze out until the temperature drops below ~ 20 – 30 K. Moving vertically away from the midplane, a freeze-out transition will occur at increasingly larger radii since the same temperature is achieved further from the star. This leads to a two-dimensional 'snow surface' which reflects the ice-gas transition for a given molecule at all radii and elevations in the disk (Fig. 3). The positions of snow lines will vary from disk-to-disk depending on, for example, the stellar mass, and will also change as the disk temperature structure evolves during the disk lifetime.

4.2.1 Deriving snowline locations

It is often difficult to measure snowline locations directly. For example, a depletion of CO in the outer disk midplane is hard to observe (except when the disk is viewed edge-on) because gas-phase CO remains abundant in higher vertical layers. Therefore, chemical effects have been used instead to estimate snowline locations. For example, N_2H^+ forms through the reaction between N_2 and H_3^+ , and is primarily destroyed by CO. N_2H^+ is therefore abundant where CO is absent from the gas (beyond the CO snowline) and where N_2 is present in the gas (inside the N_2 snowline). Because the N_2 snowline is slightly further out than the CO snowline, this results in ring-shaped N_2H^+ emission where the inner radius is roughly associated with the CO snowline (Fig. 7). Similarly, as gas-phase H_2O is the main destroyer of HCO^+ in the disk midplane, HCO^+ can be used to trace where H_2O has frozen out.

4.2.2 Importance of snowlines

Snowlines have significant consequences for the chemistry of planet formation. First, molecule freeze-out significantly lowers the available molecules for gas-phase reactions, while increasing the inventory of molecules available for ice-phase chemistry. Since different types of reactions occur in the gas versus ice, snowlines will affect what new chemistry may occur at a given disk location. Snowlines also alter the total abundance of volatile elements in the gas versus ice phase. For instance, the freeze-out of abundant species like H_2O , CO_2 , and CO can significantly increase the total amount of oxygen in the ice (and decrease the amount in the gas). This will in turn impact the composition of planetary cores and atmospheres that form from the disk solids and disk gas, respectively, in a particular disk location. The influence of disk snowlines on the elemental ratios of planet-forming material is posited as a way to connect observable properties of exoplanets (e.g. atmospheric C/O ratios) to their formation origins (Öberg et al., 2011). Snowlines will also regulate what molecules are present in icy planetesimals (like modern-day asteroids and comets), and therefore what volatile inventory could potentially be delivered via impacts to planetary surfaces.

Snowlines are also important for planet formation physics. For instance, freeze-out of certain molecules may increase the stickiness of ice-coated grains compared to bare grains, increasing the efficiency of dust growth and in turn promoting the first steps of planet formation. Just interior to snowlines, slight increases in the gas pressure can also cause local pile-ups of dust, again promoting particle growth.

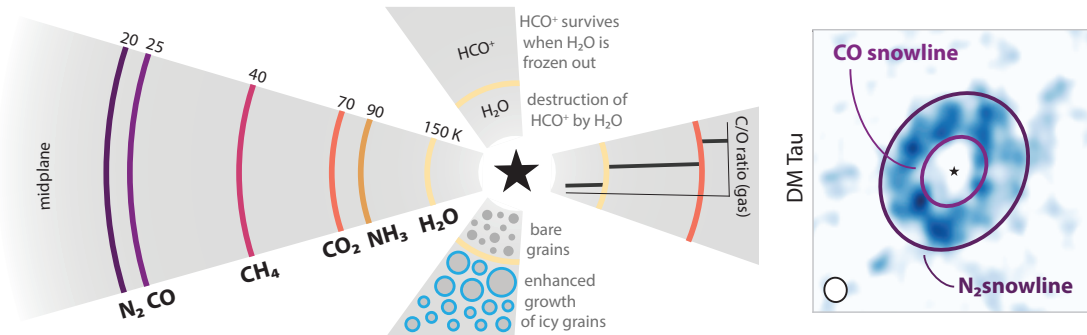


Fig. 7 Illustration of snowlines. Left: Schematic of different snowline locations in the disk midplane, and examples of their effects on the disk chemical and physical structure. The left sector shows the snowline locations of the main carbon, oxygen and nitrogen carriers. Indicated freeze-out temperatures are approximate and depend on the density and the composition of the existing ice layer. The bottom sector displays the effects of the water snowline on the dust grains. The right sector presents a simplified view of how the carbon-to-oxygen (C/O) ratio of the gas changes across the H₂O and CO₂ snowlines (based on Öberg et al. 2011). The top sector illustrates how chemistry can be used to locate snowlines, as depicted for the H₂O snowline. Right: The CO and N₂ snowlines are traced by the inner and outer edge, respectively, of a bright N₂H⁺ emission ring as N₂H⁺ is formed from gaseous N₂ and destroyed by gaseous CO (adapted from Qi et al. 2019 with permission; ©AAS). The ellipse in the lower left corner marks the synthesized beam-size of the interferometric observations, indicating the spatial resolution.

4.3 Young disks

The chemistry of young disks that are still surrounded by remnants of the envelope ($\lesssim 0.5 - 1$ Myr old) have not yet been studied in as much detail as those of more-evolved mature protoplanetary disks. While the overall chemical structure as described above is expected to be present, there are already some notable differences observed between young protostellar disks and mature protoplanetary disks. For example, young disks are typically warmer due to higher mass accretion rates and the presence of an envelope, which results in the snowlines being at larger radii from the star. In particular, young disks smaller than $\lesssim 100$ au appear to have no CO ice, with CO freezing out only in the envelope beyond the disk (van 't Hoff et al., 2020). Another topic of recent research is whether the accretion of material from the envelope onto the young disk can create a shock, and whether this has a chemical signature (e.g., Sakai et al., 2014). The sulfur-bearing species SO and SO₂ have been postulated as good tracers of such accretion shocks, and while SO emission has been observed around the disk-envelope interface for a few systems, how uniquely these molecules are associated with a shocked region remains undetermined.

5 Elemental budget

Tracking the volatile elements H, C, O, N, S, and P is of particular interest due to their universal importance in terrestrial biochemistry. In planet-forming environments, these elements can be speciated into different molecular carriers, which may be partitioned into either the solid or gas phase depending on their volatility. For instance, at temperatures around 50 K, carbon stored in CO will exist as a gas, while carbon stored in CO₂ will exist as a solid. The incorporation of the biogenic elements into planets therefore involves (i) the chemical processes that set the relative abundances of different molecular carriers, and (ii) the sublimation behavior which regulates the gas versus ice partitioning of each molecule.

5.1 Hydrogen

Hydrogen makes up the vast majority of interstellar material (74% of the entire mass budget). In dense star-forming regions (including disks), most H is in the form of H₂, which is quite chemically inert. Hydrogen is incorporated into molecules early in the star-formation sequence, resulting in the formation of hydrides like H₂O, NH₃, CH₄, CH₃OH, and other organics. In ices, these molecules account for much of the H budget, because due to its high volatility, H₂ will not be retained in the solid state.

The bulk of the disk mass is thus composed of H₂, and H₂ is also expected to dominate the composition of primordial planetary atmospheres. Because H₂ has no permanent dipole moment, it is not observable in cold environments (see more in Sect. 9.1). This means that the mass of a disk, and therefore the amount of material available to form planets, cannot be measured directly. The best alternative tracer of the gas mass is the deuterated form of H₂, HD (see more in Sect. 6.1). However, suitable transitions fall in the far-IR and are not observable with current facilities. Gas masses are therefore often estimated either from the dust mass obtained from the continuum emission assuming a gas-to-dust ratio of 100, or from optically thin CO isotopologue emission adopting interstellar values for the isotope ratios and the CO abundance with respect to hydrogen (10^{-4}).

5.2 Carbon & Oxygen

The main volatile carbon carriers in protoplanetary disks are CO and CO₂, while O is mainly partitioned into H₂O, CO₂, and CO. Other C- and O-bearing volatiles are low in abundance compared to CO, CO₂, and H₂O, and therefore less important to the bulk elemental compositions of planet-forming gas and solids. Roughly 50% of the cosmic C budget, and a few tens of percent of the O budget, are expected to be stored in a refractory form, i.e. minerals, amorphous carbon or macromolecular organics.

In the cool, outer regions of protoplanetary disks, CO and H₂O appear to be ‘depleted’ from the gas in the observable surface layers of the disk, by factors of 10–100 compared to the interstellar budgets (e.g., Ansdell et al., 2016; Du et al., 2017). CO₂ is not directly observable in cool disk gas due to having no rotational transitions (see Sect. 9.1). This depletion is thought to reflect the coupled chemistry and dynamics within the disk: as ice-covered grains grow in size, they gravitationally settle and bring icy material (dominated by H₂O and CO) to the midplane. This volatile material may be prevented from re-entering the gas by some combination of chemical reprocessing into less volatile material, physical sequestration in large solid bodies, and drift inwards towards the star. The net effect is that oxygen and, to a lesser extent carbon, are removed from the gas in elevated layers of the disk. Moreover, grain growth removes small dust from the disk atmosphere, allowing more UV radiation to penetrate into the molecular layer of the disk and driving photochemical processes.

Other chemical indicators tell us that oxygen must be more depleted than carbon: the relatively high gas-phase abundances of hydrocarbons (C₂H, cyclic-C₃H₂) and nitriles (CN, HCN, HC₃N, CH₃CN) necessitate a high carbon-to-oxygen ratio in the gas (e.g., Bergin et al., 2016; Le Gal et al., 2019). One way to increase the gas C/O ratio is photodissociation of CO, the main gas-phase carbon carrier, followed by H₂O formation from the free oxygen. However, this process can only achieve C/O ratios as high as unity, whereas ratios around 1.5–2 are implied by the bright hydrocarbon emission. Photoablation of carbon grains in the UV-irradiated disk surface has been suggested as an additional source of carbon to achieve C/O ratios >1 (Bosman et al., 2021). While CO does not appear to be depleted in young disks, nondetections of water emission suggest that the abundance is low (Harsono et al., 2020). Depletion of water may thus already occur during the embedded phase.

Volatile C and O that is sequestered on icy pebbles in the midplane is likely subject to further transport in the disk. As mentioned in Section 2, pebble drift causes solids to spiral inwards towards the star, except when drift is halted by the presence of substructures (pressure ‘bumps’). There is mounting evidence that, for systems with unhindered drift (small, smooth disks), the inner disk is strongly enriched in volatile gas, interpreted as a signature from the drift and sublimation of icy material originating in the outer disk (e.g., Banzatti et al., 2023). On the other hand, for systems with pressure bumps (large, sub-structured disks), it is expected that inner disks should be relatively dry and that O- and C-rich ices are accumulated at the substructure locations (e.g., Vlasblom et al., 2024). Understanding radial ice transport will be critical to inferring the reservoir of volatiles available to planets forming at different distances from the host star in systems with different physical substructures.

5.3 Nitrogen

Constraints on the total disk nitrogen budget are more limited. N₂ is suspected to be the dominant volatile N carrier, but it is undetectable as a homonuclear diatomic (see Section 9.1). Observations of trace N carriers must be used instead to follow the nitrogen chemistry—in the gas phase, this includes protonated N₂ (N₂H⁺), nitriles (CN, HCN, HC₃N, CH₃CN), and in very few cases ammonia (NH₃). Disks appear to be especially efficient sites for nitrile formation, and HCN is commonly detected both in the cool outer disk and the hot inner disk. Currently, there is no evidence that chemical–dynamical evolution affects the disk nitrogen budget as it does the C and O budget. One possible explanation is that the major N carrier, N₂, is quite volatile and chemically inert, meaning that it is not susceptible to sequestration on grains either by freeze-out or by processing to a less volatile carrier. There are currently few constraints on the ice-phase N budget in disks, though some clues come from solar system comets. Low cometary nitrogen abundances have long puzzled the community, though in recent years it has emerged that much of the solid N budget may be in the form of semi-refractory NH₄⁺ salts, which form through thermal reactions between NH₃ and ice-phase acids like H₂S, HCOOOH, and HCN (Poch et al., 2020). Early JWST observations of protoplanetary disk ices show hints of ammonia-H₂O hydrates and OCN⁻, but as of 2024 there have been no claims of NH₄⁺ nor other trace N carriers like HCN (e.g., Sturm et al., 2023).

5.4 Sulfur

Several gas-phase sulfur carriers have been detected in disks: CS, SO, H₂S, H₂CS, and SO₂. However, these gas-phase carriers still represent just a small fraction of the cosmic S budget (Keyte et al., 2024), which is also the case for protostellar systems. Of the (trace) gas-phase carriers, there are hints that a surprisingly high fraction may be in an organic form like H₂CS. Much of the S reservoir is expected to be locked in refractory grains, an idea supported by relatively high S abundances in stellar photospheres which reflect freshly accreted solids (Kama et al., 2019). While OCS ice has been tentatively found in JWST disk observations (Sturm et al., 2023), the total S inventory in ice appears also insufficient to explain the full S budget, implying a larger contribution of mineral forms of sulfur. Interestingly, while H₂S is the dominant ice-phase S reservoir in comets, it has yet to be detected in the ice phase either in disks or in earlier stages of star formation.

5.5 Phosphorus

The phosphorus budget in protoplanetary disks is virtually unconstrained: no detections of gas or solid-phase phosphorus carriers have been made. In prior star forming stages, gas-phase P carriers are only detected in shocked regions, implying that most of the P reservoir is locked in refractory minerals (Bergner et al., 2022). Given the non-detection of any gas phase P tracer in disks, it is likely that most P is similarly stored in refractory grains. In the solar system, the phosphorus carrier PO was detected in the coma of comet 67P (Rivilla et al., 2020), so a trace volatile P component may also be present but remaining undetected in other systems.

6 Isotopes

Isotope fractionation is the preferential enrichment or depletion of a particular isotope in a molecular reservoir relative to the cosmic isotope ratio. Isotopes are different ‘versions’ of an element due to different numbers of neutrons in their nuclei. For example, the main isotope of carbon is ^{12}C , with ^{13}C being a factor ~ 70 less abundant in the local ISM (Wilson & Rood 1994). Molecules that incorporate different isotopes are called isotopologues (e.g., CO isotopologues include $^{12}\text{C}^{16}\text{O}$, $^{13}\text{C}^{16}\text{O}$, $^{12}\text{C}^{18}\text{O}$). Fractionation is sensitive to the physical conditions in which a molecule formed, such as temperature, radiation field, and ionization rate. Molecular isotope ratios are therefore diagnostic of the origin of molecules within interstellar settings. For example, fractionation is often particularly effective at low temperatures due to the small, but non-zero, zero point energy. This is the minimum energy a molecule can have based on quantum mechanical principles. The zero point energy depends on the mass of the molecule, and is lower for an isotopically heavier molecule (e.g., ^{13}CO) compared to an isotopically lighter variant (^{12}CO). The incorporation of a heavier isotope into a molecule can thus result in the release of energy, while the reverse reaction requires energy. At temperatures below the zero point energy difference, enrichment with the heavier isotope is therefore favored. Fractionation signatures observed in protoplanetary disks may be inherited from prior stages of star formation, or reflect in situ chemical processes.

6.1 Deuterium

The less abundant stable isotope of hydrogen is called deuterium and instead of the ^2H notation as used for other elements, this isotope is denoted D. Deuterium was formed in the big bang and has a cosmic abundance of roughly 10^{-5} with respect to hydrogen. Deuterium fractionation is initiated by the exchange reaction $\text{H}_3^+ + \text{HD} \leftrightarrow \text{H}_2\text{D}^+ + \text{H}_2$, where the backward reaction is slightly endothermic (i.e., requiring energy) and therefore the forward direction is heavily favored at low temperatures. Deuterium can then be transferred from H_2D^+ to other molecular carriers, resulting in enhanced molecular D/H ratios. Due to the relatively large mass difference between H and D, the difference in zero point energy results in very strong fractionation effects in cold star-forming environments, with molecular D/H ratios up to a few thousand times higher than the cosmic D/H ratio. Deuterium fractionation can also operate at somewhat higher temperatures (>30 K), via $\text{CH}_3^+ + \text{HD} \leftrightarrow \text{CH}_2\text{D}^+ + \text{H}_2$. Both low-temperature and high-temperature fractionation pathways are inferred to be at play in the outer and inner disk regions, respectively. Deuterated molecules detected in protoplanetary disks are DCO^+ , DCN , N_2D^+ , and C_2D .

While there are no direct constraints on ice-phase deuteration levels within protoplanetary disks, high deuteration levels are seen in cometary ices in the modern-day solar system. In particular, the high $\text{D}_2\text{O}/\text{HDO}$ ratio in comets cannot be explained by in situ disk chemistry, and is inferred to reflect the inheritance of pre-stellar icy material. Indeed, D/H is enhanced relative to the solar D/H in most rocky and icy solar system bodies, but to varying degrees, suggesting a balance between inherited and reprocessed reservoirs of solid hydrogen carriers (e.g. H_2O , organics) during the assembly of planetesimals. D/H ratios in the solar system giant planets are close to the solar D/H ratio, implying that the parent disk gas did not experience significant fractionation.

6.2 Oxygen and Nitrogen isotopes

The main oxygen and nitrogen isotopes are ^{16}O and ^{14}N , respectively, with ^{18}O , ^{17}O , and ^{15}N less abundant in the local ISM compared to the main isotopes by factors of ~ 560 , ~ 1790 , and ~ 450 , respectively (Wilson and Rood, 1994). Due to their higher mass, the relative mass difference between different isotopes is small, and kinetic chemical effects at low temperatures, as observed for H and D, are minimal. Instead, oxygen and nitrogen fractionation primarily proceed via a photodissociation mechanism. The major gas-phase carriers CO and N_2 undergo photodissociation via discrete line transitions and can therefore self-shield (see Sect. 4.1 and Fig. 5). Rare isotopologues are less abundant, and therefore a longer path length is required before the dissociating radiation is fully absorbed. There exist regions where main isotopologues are already self-shielding, while minor isotopologues are efficiently dissociated, freeing the rarer isotope for incorporation into other molecules (Fig. 5). For instance, $^{14}\text{N}^{14}\text{N}$ will self-shield closer to the edge of a cloud compared to $^{15}\text{N}^{14}\text{N}$, resulting in enrichment of ^{15}N within photochemical products like CN and HCN. Similarly, CO will self-shield before C^{18}O , enhancing the production of H_2^{18}O over H_2^{16}O . Photodissociation fractionation is expected to be important in disks given the strong UV field in the surface layers. There is evidence for an increasing $\text{HC}^{14}\text{N}/\text{HC}^{15}\text{N}$ ratio moving from the inner to outer region of a protoplanetary disk, consistent with enhanced photodissociation in the less-shielded outer disk (Hily-Blant et al., 2019). ^{18}O enrichment in primitive solar system solids is similarly thought to reflect isotope-dependent photodissociation, though it remains debated whether the fractionation occurs during the disk stage or is inherited from the molecular cloud.

6.3 Carbon isotopes

Carbon may be fractionated either via a photodissociation mechanism, or a low-temperature exchange mechanism. CO is the main gas-phase carbon carrier and, as noted above, is subject to self-shielding effects which should enrich photochemically produced molecules with ^{13}C relative to ^{12}C . The slightly endothermic exchange reaction $\text{CO} + ^{13}\text{C}^+ \leftrightarrow ^{13}\text{CO} + \text{C}^+$ is also expected to operate at temperatures <40 K, but requires high ionization rates to be an efficient fractionation pathway. Observations of carbon fractionation in protoplanetary disks hint at the existence of two distinct carbon isotope reservoirs: hydrocarbons (e.g. C_2H) appear enhanced in ^{12}C , and CO in ^{13}C (Yoshida et al., 2022; Bergin et al., 2024). Several early measurements of fractionation in exoplanet atmospheres indicate strong ^{13}C enrichments, which would require the accretion of ^{13}C -enriched gas from the disk. On the other hand, there are no strong signatures of carbon fractionation in the solar system. $^{13}\text{CO}_2$ has been detected in both disk ices and hot inner-disk gas with JWST (Grant et al., 2023; Sturm et al., 2023), but due to the high optical depth of $^{12}\text{CO}_2$, extracting isotope ratios will be challenging. Additional measurements of carbon fractionation in different disk gas reservoirs as well as exoplanet atmospheres are needed to provide more clarity on the importance of carbon isotope fractionation within disks.

7 (Complex) organic molecules

There is great interest in understanding the inventory of organic material available to seed forming planetesimals and planets with potential building blocks for prebiotic chemistry. Given the energetic conditions associated with active planet formation, molecules are not expected to survive direct incorporation into planets; instead, delivering molecules intact to terrestrial planets likely requires post-formation impacts of icy planetesimals. In planet-forming environments it is thus the organic content of the ice that matters for terrestrial planets, but given the difficulties identifying complex molecules in ices (see Section 9), gas-phase studies are crucial to uncover the full organic reservoir.

7.1 Outer disk gas

At millimeter wavelengths, the small organics HCN, C₂H, and H₂CO are commonly detected in protoplanetary disk gas. HCN and C₂H are thought to form primarily through in situ gas-phase chemistry. The abundances of these species are well correlated in disks (Bergner et al., 2019), likely reflecting that both are photochemically produced in C-rich gas. H₂CO may form on grains in the outer disk beyond the CO snowline, or via warm gas-phase chemistry interior to the CO snowline. The total inventory of small organics in disks is inferred to be quite large, equivalent to tens to hundreds of Earth oceans per disk (Öberg et al., 2021).

The larger molecules *c*-C₃H₂ (cyclic cyclopropynylidene), HC₃N (cyanoacetylene), and CH₃CN (methyl cyanide) are also commonly detected in cool disk gas (Ilee et al., 2021). Meanwhile, CH₃OH (methanol), the most abundant organic in the preceding protostellar stage, has proved surprisingly challenging to detect in disks (Walsh et al., 2016). Indeed, CH₃CN/CH₃OH ratios in disk gas are ~2 orders of magnitude higher than protostellar values, implying a dramatic shift in the organic chemistry during the disk stage. This is likely another ‘symptom’ of the phenomenon discussed in Section 5.2: grain growth and disk dynamics sequester O-rich ices in the midplane, leaving behind an O-poor gas exposed to high levels of UV radiation. CH₃CN and HC₃N are shown to form efficiently via photochemistry operating in O-poor gas, and may therefore serve as signposts for the general reshaping of the disk volatile reservoir (Calahan et al., 2023). The efficient synthesis of nitriles during the disk stage is intriguing due to the particular importance of nitriles within prebiotic chemical reaction networks. Complex nitrile emission appears to originate close to the disk midplane, supporting that these molecules are available near the site of planet formation.

In recent years, the detection of larger, O-bearing organics in disks has been enabled by focusing on young, outbursting disks as well as more massive Herbig systems. The disk V883 Ori is an archetypical outbursting system: the disk has been transiently heated by an accretion burst, pushing the H₂O snowline out to ~80 au (compared to ~1 au in a typical T Tauri disk). A rich array of complex organics (e.g., acetaldehyde: CH₃CHO, methyl formate: CH₃OCHO, acetone: CH₃COCH₃) have been detected in the gas of the V883 Ori disk (Fig. 8; Lee et al. 2019), implying that organics are abundant in disks but are typically hidden in the icy midplane. Meanwhile, disks around Herbig stars are warmer than T Tauri disks, and complex organics (e.g. methanol: CH₃OH, dimethyl ether: CH₃OCH₃, ethylene oxide: *c*-H₂COCH₂), have now been detected towards several such systems (e.g., Booth et al., 2021). Importantly, these disks are expected to be too warm for CO to freeze out; since ice-phase CO is typically a requisite ingredient for CH₃OH formation, the detection of CH₃OH towards these systems necessitates inheritance of icy material into the disk.

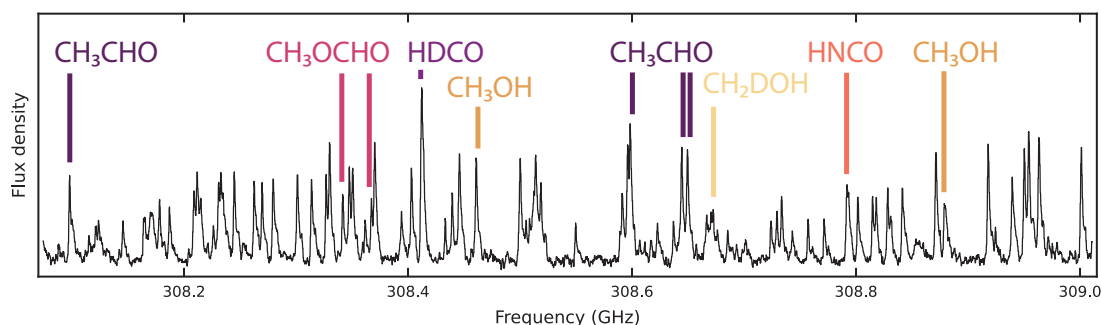


Fig. 8 Spectrum toward the disk around the outbursting young star V883 Ori displaying a wealth of emission lines from complex organic molecules. Several of the observed lines are annotated as an example. Data from the ALMA Large Program COMPASS (PI: Jes Jørgensen).

7.2 Inner disk gas

Some small organics and hydrocarbons are detected at IR wavelengths tracing hot inner-disk gas from within the water snowline: HCN, C₂H₂, and CH₄. From the Spitzer era, it was found that HCN/C₂H₂ ratios are systematically lower in disks around lower-mass M dwarf systems compared to solar-like systems (Pascucci et al., 2013). There are hints that the nitrile/hydrocarbon ratios are also lower in the outer disks of M dwarf systems. Possible explanations include the distinct radiation field of M dwarf versus T Tauri stars, or differences in the efficiency of icy pebble drift depending on disk mass. JWST has recently detected a remarkable complex chemistry in the inner disk around

very low mass M dwarf stars, including large hydrocarbons (ethylene: C_2H_4 , benzene: C_6H_6) as well as the nitrile HC_3N (Tabone et al., 2023). This chemistry requires high C/O ratios and may reflect efficient destruction of carbon-rich grains in the inner disk (Li et al., 2021), and/or the trapping of O-rich icy pebbles further out in the disk that leaves the inner disk O-poor (e.g., Mah et al., 2024). The importance of the so-called ‘soot line’ (location where carbon-rich grains are thermally destroyed) to disk organic chemistry should become clearer with improved demographics of inner-disk chemistry with JWST.

7.3 Ices

Organic molecules have not yet been detected in the ice-phase of protoplanetary disks, though the first JWST disk ice spectrum revealed hints of OCN^- and OCS (Fig. 9; Sturm et al. 2023). Based on protostellar ice measurements and disks with active ice sublimation (e.g. V883 Ori), disk ices are expected to carry a wealth of organic complexity. Indeed, solar system comets host an incredibly diverse assortment of organic molecules, including biologically relevant molecules like glycine (the simplest amino acid). Meteorites contain significant quantities of macromolecular organic matter, which likely began as icy material that was subject to heavy radiation/thermal processing. The extent to which cometary and meteoritic organics reflect inherited prestellar/protostellar chemistry versus in situ disk ice processing remains an open question. The agreement between the relative abundances of organics in the inner region of protostellar envelopes (called ‘hot corinos’ for low-mass protostars and ‘hot cores’ for high-mass protostars), outbursting protostellar disks, and comets is suggestive that the ice composition from early star-forming stages may be inherited relatively intact to the stage of icy planetesimal formation (Drozdovskaya et al., 2019). Additional ice-phase organic molecule formation and/or reprocessing may also occur during the disk stage, particularly if icy grains are efficiently transported to moderately elevated, UV-rich layers of the disk, or in cases with high midplane ionization levels.

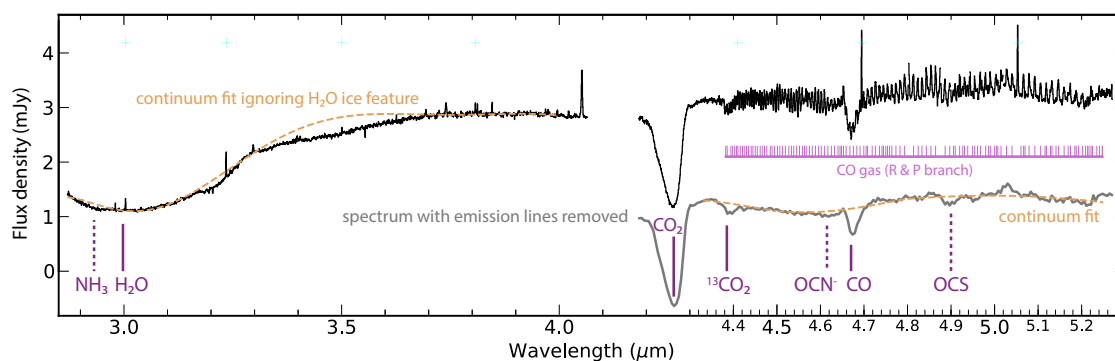


Fig. 9 JWST/NIRSpec spectrum of the edge-on disk HH 48 NE from the Early Release Science program Ice Age (black). The spectrum between 4.2 and 5.3 μm after removal of the gas emission lines is shown with a vertical offset (gray). The CO ro-vibrational emission lines are marked with light purple lines, and the ice absorption features with dark purple lines. Dotted lines indicate tentative detections. A local continuum fit excluding the CO_2 and broad H_2O ice features is shown with an orange dashed lines to highlight the tentative NH_3 , OCN^- and OCS ice features. Adapted from Sturm et al. (2023); ©ESO.

8 Chemical substructure

Since the advent of ALMA, it has become possible to spatially resolve the emission from protoplanetary disks at (sub-)millimeter wavelengths. This led to the discovery that the dust is not smoothly distributed in most disks, but often exhibits rings, gaps, and spirals—so-called ‘substructures’. While the origin of these substructures is not definitively known, they are commonly thought to be associated with sites of active planet/planetesimal formation. More recently, rings and gaps have been found to be ubiquitous for gas molecules as well (Fig. 10; Öberg et al. 2021). Chemical substructures show a remarkable diversity, with a range of morphologies observed both for different molecules imaged within the same disk, and for the same molecule imaged in different disks.

The origins of chemical substructures remain murky. Snowlines (CO , N_2) have largely been ruled out as an explanation. In some cases, gas substructures are found to either correlate or anti-correlate with the presence of dust substructures, but there is no universal trend (Law et al., 2021). Because chemistry is sensitive to a variety of factors (e.g. temperature, radiation field, gas density), it may be that these driving factors combine in various ways to produce a range of outcomes for different molecules in different systems. Identifying trends more definitively will require high-resolution chemical observations towards numerous additional disks. Ultimately, this is a topic of pressing importance to predicting planetary compositions, since chemical substructuring means that planets forming in different disk locations could accrete quite different gas compositions. Moreover, if there is indeed an association between dust and gas substructure, then the very process of planet formation may be reshaping the chemical composition in the neighborhood of the forming planet.

In addition to large-scale gas substructures, the high spatial and spectral resolution of ALMA has allowed the discovery of localized structures in individual frequency channels toward a few disks (Fig. 11, left panels). These so-called ‘kinks’ are believed to be due to

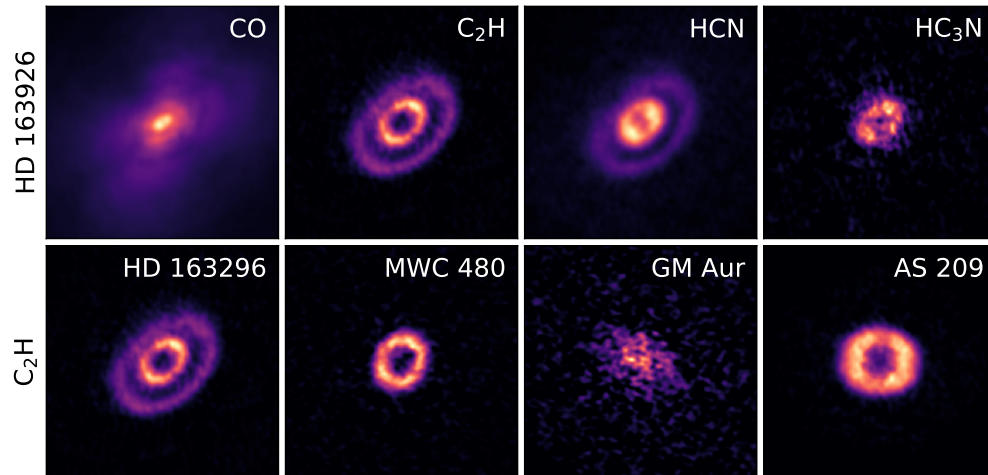


Fig. 10 Illustration of diversity in chemical substructure seen towards protoplanetary disks, made using data from the MAPS ALMA large program (Öberg et al., 2021). Top: Different molecules imaged towards the HD 163296 disk. Bottom: C_2H imaged towards different disks.

(forming) planets that locally perturb the gas. Such perturbations can also be seen in the overall velocity profile of the disk as small deviations from Keplerian rotation (Fig. 11, right panel). While these types of studies require very high signal-to-noise data, they may be one of the best ways to detect young planets embedded in disks.

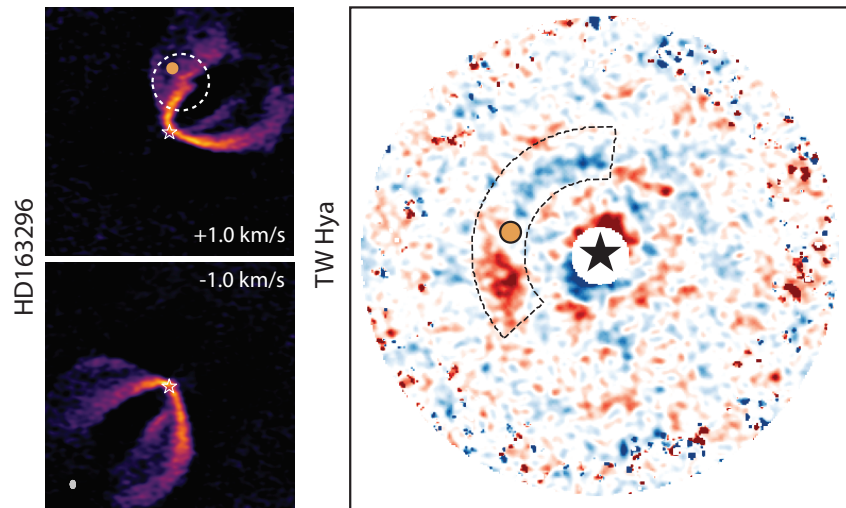


Fig. 11 Illustration of different techniques to infer the presence of planets through deviations in the velocity pattern using molecular line observations. The velocity deviations are marked by dashed regions and the inferred location of the planets are marked by orange circles. Left: A localized disturbance in the Keplerian pattern ('kink') of CO emission is visible in the northwestern side of the HD 163296 disk at redshifted velocities around 1.0 km/s (dashed contour in top panel), while a normal Keplerian pattern is visible at the same blueshifted velocities arising from the southeastern part of the disk (bottom panel). Figure adapted with permission from Pinte et al. (2018); ©AAS. Right: Deviations from Keplerian velocity (dashed contour) in TW Hya stand out as strong residuals when the expected Keplerian velocity structure of the disk is subtracted from the observed velocity map for CS. Figure adapted from Teague et al. (2018); ©AAS.

9 Observing molecules in disks

Molecules in disks, and astronomical environments in general, can be observed through their interaction with electromagnetic radiation. A given molecule can only emit or absorb radiation at particular frequencies corresponding to energy differences between two quantized energy levels. Molecules have quantized electronic states, vibrational states and rotational states. As depicted in Figure 12, each electronic state contains many vibrational states, each of which contains many rotational states. Observations of molecules in disks rely predominantly on transitions between rotational and vibrational states: electronic transitions have wide spacings between energy levels, and are typically not populated at the relatively low temperatures ($\lesssim 1000$ K) typical of protoplanetary disks. For most astrophysically relevant molecules, rotational transitions lie in the microwave (centimeter, millimeter and submillimeter wavelengths), and vibrational transitions in the infrared. Current (sub)millimeter facilities commonly used to observe disks are ALMA (the Atacama Large Millimeter/submillimeter Array), NOEMA (the NOthern Extended Millimeter Array) and the SMA (the Submillimeter Array). Infrared observations are best done from space, which is currently only possible with JWST (the James Webb Space Telescope), but some wavelength ranges are also accessible from the ground, with for example the VLT (Very Large Telescope) and the future ELTs (Extremely Large Telescopes).

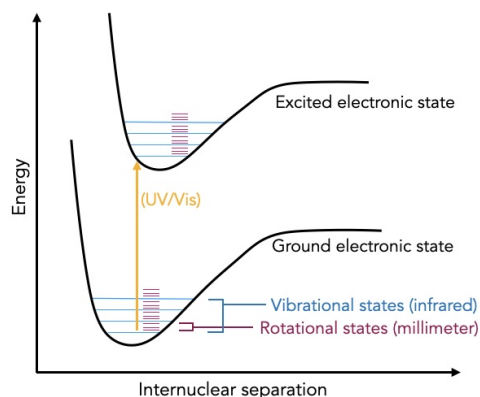


Fig. 12 Summary of molecular energy levels. Each electronic state contains numerous vibrational states, which in turn contain many rotational states. The large energy spacing between electronic states corresponds to transitions in the UV/visible, whereas vibrational transitions typically occur in the infrared, and rotational transitions in the millimeter.

9.1 Microwave observations

The lowest rotational levels have energies (E_{ul}/k_B , where k_B is the Boltzmann constant) as low as a few Kelvin, and are therefore readily excited at temperatures of only ~ 10 K. This makes rotational spectroscopy the best tool for probing emission from cold interstellar environments. Millimeter observations are also exceptionally sensitive and can detect molecules with low abundances down to $\sim 10^{-11}$ with respect to H_2 . One limitation is that rotational transitions can only be observed for gas-phase molecules, as the interactions between molecules in ice lattices hamper rotations. Rotational transitions are also only possible for molecules that possess a permanent electric dipole moment. The electric dipole moment is a measure of the imbalance of charge within a molecule. Such an imbalance is required to produce an electric field that can couple to photons. Homonuclear molecules such as H_2 and symmetric molecules like CO_2 do not have a permanent dipole moment and can therefore not be observed via pure rotational transitions.

The energy spacing between different rotational states depends on the molecular geometry. Every molecule can be classified as one of four general types of rotor, determined by the moment of inertia along each of three orthogonal spatial axes (Fig. 13). The simplest case is for a linear molecule (e.g. H_2 , CO, HCN), where one moment of inertia is equal to zero. For linear molecules, rotation can therefore be treated as a ‘rigid rotor’ (Fig. 14). Here, the rotational energy levels are given by $E = BJ(J + 1)$, where J is the rotational quantum number and B the rotational constant, which is inversely proportional to the moment of inertia of the molecule. Rotational transitions are only possible between adjacent rotational states i.e. $\Delta J = \pm 1$. The energy of a rotational transition, $\Delta E = E(J + 1) - E(J)$, is then always equal to $2B(J + 1)$. Correspondingly, the rotational transitions for linear molecules are spaced at even frequency intervals. It is clear that molecules with a larger B (i.e., lower moment of inertia; lighter or more compact molecules) have wider spacing between energy levels, and transitions at higher frequencies. Similarly, molecules with a smaller B (i.e., higher moment of inertia; heavier or larger molecules) have more closely spaced transitions that fall at lower frequencies.

Spherical tops (e.g. CH_4) have three identical moments of inertia, and exhibit similar energy spacing as linear molecules. Symmetric tops have two identical moments of inertia and one axis with a different moment of inertia, and can be either prolate (cigar-shaped, e.g. CH_3CN) or oblate (pancake-shaped, NH_3). In this case, two rotational quantum numbers are needed to describe the rotational states: J and K . J is the rotational quantum number (as before), and K is the quantum number associated with the projection of the rotational angular momentum onto the symmetry axis, with $K \leq J$. The selection rule for transitions is $\Delta J = \pm 1$ and $\Delta K = 0$. Because radiative transitions between K -levels are not allowed, the relative population of different K -levels is set purely by collisions, making symmetric tops excellent temperature probes. Transitions with different K quantum numbers but the same upper and lower J -levels occur close together in frequency, and are often referred to as ‘rotational ladders’. Finally, asymmetric tops are molecules for which all three orthogonal rotational axes have different moments of inertia. For such molecules (e.g. H_2O , CH_3OH) there is no simple equation representing the rotational energy levels. These

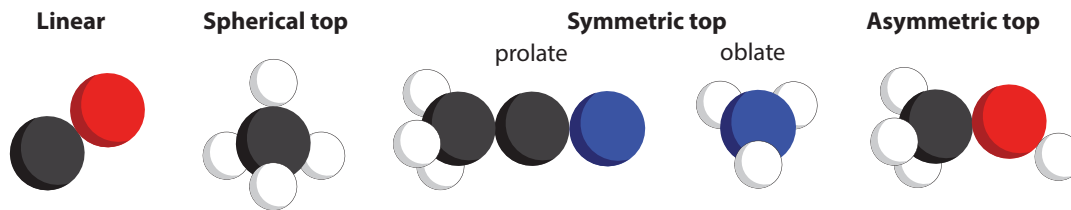


Fig. 13 Illustration of the four different molecular geometries or rotors: linear (e.g., CO), spherical top (e.g., CH₄), symmetric top, which can be either prolate (e.g., CH₃CH) or oblate (e.g., NH₃), and asymmetric tops, which are all molecules that do not fall into the previous three categories (e.g., CH₃OH).

molecules have chaotic and often very complex rotational spectra. Most molecules fall into this category.

Even small linear molecules may have a more complicated energy structures and spectra than described above due to nuclear spin effects. For nuclei with non-zero spin, interactions between the nuclei and the electrons result in so-called hyperfine splitting of the rotational energy levels. CN, HCN and C¹⁷O are examples of molecules routinely observed in disks that display hyperfine structure in their spectra. For molecules that contain two or more hydrogen atoms, such as H₂O and H₂CO, the rotational transitions are split into two ladders for molecules with either the hydrogen nuclear spins aligned parallel (ortho) or anti-parallel (para). Radiative transitions between these ortho and para states are forbidden to high order, and only chemical reactions can transform one state into the other. The ortho-to-para ratio can take values between 0 and 3. Furthermore, transitions from molecules with unpaired electrons, such as CN, can be split into multiple components in the presence of a magnetic field ('Zeeman splitting').

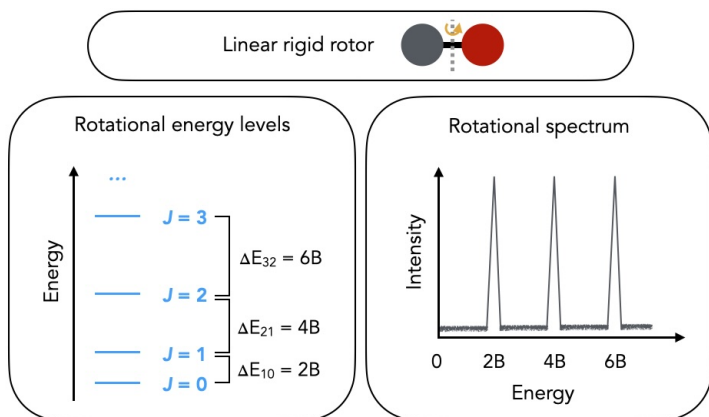


Fig. 14 Illustration of rotational energy levels for a linear rigid rotor. Energy levels are given by $BJ(J+1)$, leading to transition energies ΔE of $2B(J+1)$ (left panel). There is then a constant spacing of $2B$ between rotational transitions (right panel).

9.2 Infrared observations

The advantage of infrared observations is that vibrational transitions can be observed for molecules both in the gas and in the ice, as well as for some molecules without a permanent dipole moment. Vibrational levels are denoted by the vibrational quantum number ν . The vibrational energy levels can be approximated by a harmonic oscillator (Figure 15): $E_\nu = (\nu + \frac{1}{2})h\nu_m$, where ν_m is the fundamental frequency, proportional to the bond stiffness and inversely proportional to the reduced mass. For a perfect harmonic oscillator, only transitions with $\Delta\nu = \pm 1$ are allowed. This results in a transition energy spacing of $\Delta E = h\nu_m$, which is the same for all allowed transitions: an ideal harmonic oscillator would have a vibrational spectrum consisting of just one line at this frequency, called the 'fundamental' transition. Real molecules are not perfect harmonic oscillators, and weak 'overtone' transitions are possible with $\Delta\nu > |1|$. Anharmonicity also causes different fundamental transitions ($\Delta\nu = \pm 1$) to occur at different frequencies in real molecules.

In order for a molecular vibration to be IR-active, there must be a change in the dipole moment as a result of the vibration. This means that vibrational transitions are allowed for symmetric polyatomic molecules (e.g. CO₂, CH₄) which have no permanent dipole moment and therefore no rotational spectrum. Vibrational transitions remain forbidden for homonuclear diatomics (e.g. N₂, O₂) which have no bond dipole. For a non-linear molecule with N atoms, there are $3N - 6$ different vibrational modes (e.g., different ways in which the molecule can bend and stretch). Linear molecules have $3N - 5$ different vibrations, because they have one less degree of freedom. Not all modes lead to a distinct transition energy due to degeneracies and to IR-inactive modes.

In the gas phase, vibrational transitions are often accompanied by rotational transitions with $\Delta J = 0, \pm 1$ (ro-vibrational transitions). This leads to 3 distinct 'branches' of a vibrational transition. The R-branch refers to transitions with $\Delta\nu = \pm 1$ and $\Delta J = +1$, and the P-branch to transitions with $\Delta\nu = \pm 1$ and $\Delta J = -1$. For an ideal diatomic, the transition energies would be described $\Delta E_R(\nu, J) = h\nu_m + 2B(J+1)$ and

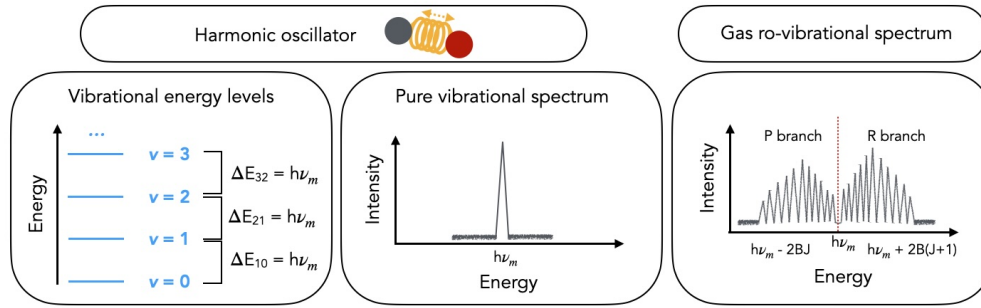


Fig. 15 Illustration of vibrational energy levels for a harmonic oscillator (left, middle panels). Energy levels are evenly spaced, leading to a single vibrational transition energy with $\Delta E = h\nu_m$. In reality, anharmonicity introduces weaker ‘overtone’ features into a vibrational spectrum. Also, vibrational transitions are often accompanied by rotational transitions, leading to a series of ro-vibrational transitions (right panel). The vertical red line marks the location where the Q branch would be if it were allowed.

$\Delta E_p(\nu, J) = h\nu_m - 2BJ$. Each line is labeled $R(J)$ or $P(J)$, where J represents the value of the lower rotational state. The Q branch refers to transitions with $\Delta\nu = \pm 1$ and $\Delta J = 0$, and is forbidden in many cases. A molecule relevant to disks that does have an allowed Q-branch is CO_2 . Because the rotational constant, B , is different in each vibrational state, the R-branch lines move closer together in the spectrum for increasing J , and eventually start moving closer to the Q-branch again. The line at the highest frequency is called the bandhead. The opposite happens for the P-branch, where the lines move further apart for increasing J .

Vibrational transitions from solid-state molecules (including ices) do not have a rotational substructure and are very broad. The line profiles depend on the morphology (i.e., crystalline or amorphous ices), the environment of the observed molecule (i.e., what other molecules are present in the ice), and the temperature of the ice. The band positions are shifted relative to the gas phase due to interactions with neighboring molecules. Ices are best observed in absorption in the near- to mid-infrared, and can therefore only be seen toward an infrared-bright background source. For disks, this means that ices have to be observed in sources with an edge-on geometry. A challenge with ice spectroscopy is the lack of specificity when identifying molecular carriers: it can be difficult to distinguish between different molecules that have the same functional group (e.g., -OH), because such a group has the same bending and/or stretching modes in different molecules. Identification is further complicated by the broad bands and environment-specific band position and profile.

10 Analysis of molecular line emission from disks

There exist many ways to extract physical parameters (e.g. column density, rotational temperature) from molecular line observations, and the appropriate analysis route depends on the observational characteristics (e.g., spatial resolution, or whether the lines are weak or strong) and the science goals. Spatially resolved observations consist of three-dimensional data ‘cubes’ with two position axes and one frequency axis. These are commonly visualized in several ways (Fig. 16). Spectra show the flux density, either in a single pixel or spatially integrated, as function of frequency or doppler-shifted velocity. Channel maps show a series of two-dimensional spatial images, each imaged at different frequencies. A ‘moment map’ is a two-dimensional image representing some statistic of the 3D cube along the spectral axis. The most common moment maps are zeroth moment (velocity-integrated intensity per pixel), first moment (intensity-weighted velocity per pixel), eighth moment (peak intensity per pixel), and ninth moment (velocity at peak intensity per pixel). For young disks, position-velocity diagrams are often used to separate emission from the disk and envelope, by presenting the emission along the major axis of the disk as function of velocity.

The signal-to-noise ratio of weak lines can be enhanced by utilizing the Keplerian velocity pattern of the disk. For example, a ‘Keplerian mask’ including only pixels expected to contain emission from the disk can be used when creating moment maps (Salinas et al., 2017), and a ‘shift-and-stack’ technique whereby the velocity of each pixel is shifted to the rest frequency can enhance signal-to-noise in line spectra (Yen et al., 2016). Finally, matched-filtering can be used to search for very weak emission lines using a strong line or model line profile as a template (Loomis et al., 2018).

Often, line emission is converted into a molecular column density (N) using the relation

$$\frac{4\pi F\Delta\nu}{A_{ul}\Omega hc g_u} = \frac{N}{Q(T)} e^{-E_u/k_B T}, \quad (1)$$

where $F\Delta\nu$ is the velocity-integrated flux, Ω is the solid angle subtended by the source, A_{ul} is the Einstein A coefficient of the transition, E_u and g_u are the energy and degeneracy of the upper level, respectively, T is the temperature of the emitting material, $Q(T)$ is the molecular partition function at temperature T , h is the Planck constant and c is the speed of light. For weak lines or spatially unresolved observations, the emission is typically integrated over the entire disk area resulting in ‘disk-integrated column densities’. When the signal-to-noise is high enough, radial column density profiles may be extracted.

The above calculation assumes that the material is in local thermodynamic equilibrium (LTE), that is, that the density is high enough for

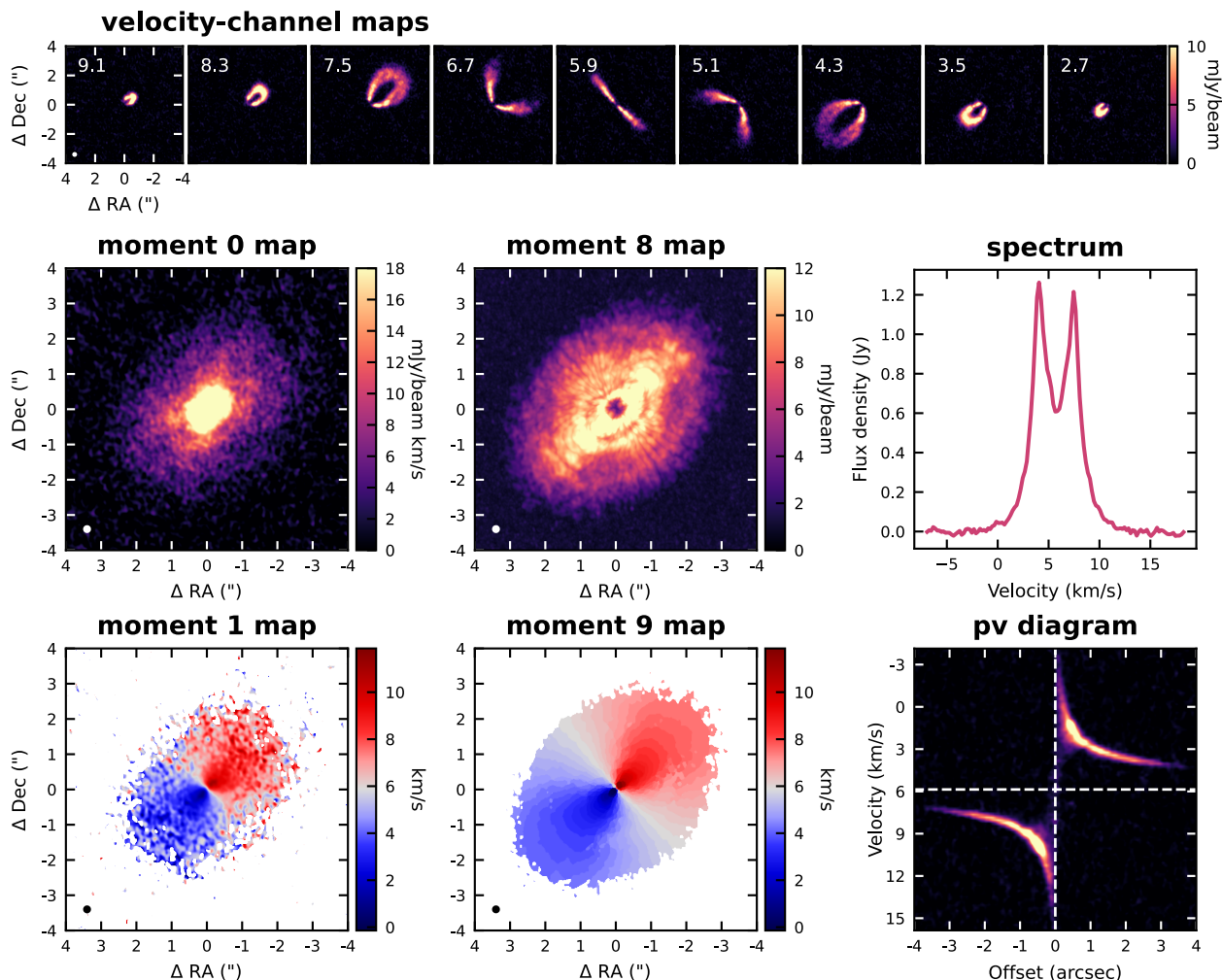


Fig. 16 Examples of different ways to display molecular line observations using C^{18}O observations of the HD 163296 disk from the ALMA Large Program MAPS (Öberg et al., 2021). Top row: Selected velocity-channel maps with the velocity (km s^{-1}) indicated in the top left corner. Middle row: Moment 0 map (velocity integrated intensity), moment 8 map (peak intensity), and spectrum or line profile (disk-integrated intensity). Bottom row: Moment 1 map (intensity-weighted velocity), moment 9 map (velocity at peak intensity) and position-velocity (pv) diagram along the disk major axis (i.e., from northwest to southeast). The colorscale of the pv diagram is the same as for the moment 8 map. The small ellipse in the bottom left corner of the velocity-channel maps and moment maps represents the synthesized beam size of the interferometric observations.

the population of the different energy levels to be determined by collisions. This is determined by a molecular transition’s ‘critical density’: the density, at a given temperature, at which the rate of collisional excitation to the upper level of the transition equals the rate of radiative de-excitation back into the lower level. If the density is below the critical density (non-LTE conditions), the balance between collisional excitation, collisional de-excitation and radiative de-excitation has to be calculated explicitly. Typically, LTE is a valid assumption when analyzing disk emission. The above relation (Eq. 1) also requires the emission to be optically thin. Observations of multiple isotopologues are often used to assess the optical depth of the emission as the flux ratio of the same transition for different isotopologues should equal the isotope ratio in case of optically thin emission. Finally, the temperature of the emitting material can be determined if multiple transitions of a given molecule are observed using the ratio of the different line intensities. In this case, temperature and column density are typically determined simultaneously. This can either be done in a ‘rotation diagram’ analysis from a linear fit to $\log(N_u/g_u)$ (which is equal to the left side of Eq. 1) versus E_u , or by fitting synthetic spectra for varying column density and temperature. If the temperature cannot be derived from the observations directly, an assumption has to be made based on other knowledge of the target.

When LTE is not valid or when one wants to derive more detailed information about the spatial distribution of a molecule, radiative transfer models can be employed to produce synthetic images for comparison with the observations. Publicly available codes exist with different degrees of complexity. For example, RADEX deals with a one-dimensional or ‘slab’ models (van der Tak et al., 2007), Ratran can be used for two-dimensional models (e.g., radial column density profiles; Hogerheijde and van der Tak 2000), and LIME and RADMC3D

can handle full three-dimensional geometries (Brinch and Hogerheijde, 2010; Dullemond et al., 2012, respectively). The input molecular distribution can also be created at different levels of complexity, ranging from simple constant abundances within varying physical regions ('parametrized' distributions) to outputs from full chemical networks. It may not come as a surprise that chemical models also vary in degrees of complexity, for example in terms of the size of the chemical network that is used, that is, the number of molecular species and chemical reactions that are included. In addition, chemical models can be separated into pure chemical models, where the chemical structure is calculated for a given input physical structure, and thermo-chemical models where the gas temperature and chemical structure are calculated self-consistently; because the chemical structure depends on the temperature and the temperature is influenced by atomic and molecular line cooling, these models incorporate an iterative process of calculating the temperature and chemical structure.

11 Future outlook

While ALMA has been operational for a little over a decade, it has not yet reached its full potential regarding studies of disk chemistry. Deep high-resolution observations of individual or small groups of disks in combination with newly developed analysis techniques are likely to reveal the chemical structure, potentially at the site where planets are forming, in unprecedented detail. Another promising avenue are 'population' studies of large numbers of disks that are now possible through Large Programs. While not (yet) as detailed as studies of individual disks, such programs will reveal global chemical properties of disks and how they change with disk evolution, as well as how chemically diverse disks really are. JWST has only just started operations and the initial results for inner disk chemistry and ice composition, as well as exoplanet atmospheres, are only just scratching the surface. At the same time, the development of more advanced chemical models incorporating more and more details of disk physics, grain growth and planet formation will provide new predictions to be tested observationally. This combination of state-of-the-art facilities (ALMA, JWST, and future ground-based Extremely Large Telescopes) and models is bound to significantly increase our understanding of planet composition in the next decade.

Acknowledgments

We would like to thank Lenore Anderson, Ted Bergin, Deniz Kaçan, Morgan Kennebeck, Vincent Kreft, Patricia Moon, William Thompson, Anna Wannemacher, and Lauren Warshaw for valuable feedback on the manuscript.

See Also: Recent in depth reviews on disk chemistry are provided by Aikawa et al. (2022) and Öberg et al. (2023).

References

- Aikawa Y and Herbst E (1999), Nov. Molecular evolution in protoplanetary disks. Two-dimensional distributions and column densities of gaseous molecules. *A&A* 351: 233–246.
- Aikawa Y, Okuzumi S and Pontoppidan K (2022), Dec. The physical and chemical processes in protoplanetary disks: constraints on the composition of comets. *arXiv e-prints*, arXiv:2212.14529doi:10.48550/arXiv.2212.14529. 2212.14529.
- Ansdell M, Williams JP, van der Marel N, Carpenter JM, Guidi G, Hogerheijde M, Mathews GS, Manara CF, Miotello A, Natta A, Oliveira I, Tazzari M, Testi L, van Dishoeck EF and van Terwisga SE (2016), Sep. ALMA Survey of Lupus Protoplanetary Disks. I. Dust and Gas Masses. *ApJ* 828 (1), 46. doi:10.3847/0004-637X/828/1/46. 1604.05719.
- Banzatti A, Pontoppidan KM, Carr JS, Jellison E, Pascucci I, Najita JR, Muñoz-Romero CE, Öberg KI, Kalyaan A, Pinilla P, Krijt S, Long F, Lambrechts M, Rosotti G, Herczeg GJ, Salyk C, Zhang K, Bergin EA, Ballering NP, Meyer MR, Bruderer S and Jdiscs Collaboration (2023), Nov. JWST Reveals Excess Cool Water near the Snow Line in Compact Disks, Consistent with Pebble Drift. *ApJL* 957 (2), L22. doi:10.3847/2041-8213/acf5ec. 2307.03846.
- Bergin EA, Du F, Cleaves LI, Blake GA, Schwarz K, Visser R and Zhang K (2016), Nov. Hydrocarbon Emission Rings in Protoplanetary Disks Induced by Dust Evolution. *ApJ* 831 (1), 101. doi:10.3847/0004-637X/831/1/101. 1609.06337.
- Bergin EA, Bosman A, Teague R, Calahan J, Willacy K, Cleaves LI, Schwarz K, Zhang K and Bruderer S (2024), Apr. The Carbon Isotopic Ratio and Planet Formation. *ApJ* 965 (2), 147. doi:10.3847/1538-4357/ad3443. 2403.09739.
- Bergner JB, Öberg KI, Bergin EA, Loomis RA, Pegues J and Qi C (2019), May. A Survey of C₂H, HCN, and C¹⁸O in Protoplanetary Disks. *ApJ* 876 (1), 25. doi:10.3847/1538-4357/ab141e. 1904.09315.
- Bergner JB, Burkhardt AM, Öberg KI, Rice TS and Bergin EA (2022), Mar. First Images of Phosphorus Molecules toward a Protosolar Analog. *ApJ* 927 (1), 7. doi:10.3847/1538-4357/ac47a2. 2201.03467.
- Booth AS, Walsh C, Terwisscha van Scheltinga J, van Dishoeck EF, Ilee JD, Hogerheijde MR, Kama M and Nomura H (2021), Jan. An inherited complex organic molecule reservoir in a warm planet-hosting disk. *Nature Astronomy* 5: 684–690. doi:10.1038/s41550-021-01352-w. 2104.08348.
- Bosman AD, Alarcón F, Zhang K and Bergin EA (2021), Mar. Destruction of Refractory Carbon Grains Drives the Final Stage of Protoplanetary Disk Chemistry. *ApJ* 910 (1), 3. doi:10.3847/1538-4357/abe127. 2101.12502.
- Brinch C and Hogerheijde MR (2010), Nov. LIME - a flexible, non-LTE line excitation and radiation transfer method for millimeter and far-infrared wavelengths. *A&A* 523, A25. doi:10.1051/0004-6361/201015333. 1008.1492.
- Calahan JK, Bergin EA, Bosman AD, Rich EA, Andrews SM, Bergner JB, Cleaves LI, Guzmán VV, Huang J, Ilee JD, Law CJ, Le Gal R, Öberg KI, Teague R, Walsh C, Wilner DJ and Zhang K (2023), Jan. UV-driven chemistry as a signpost of late-stage planet formation. *Nature Astronomy* 7: 49–56. doi:10.1038/s41550-022-01831-8. 2212.05539.
- Drozdovskaya MN, van Dishoeck EF, Rubin M, Jørgensen JK and Altwegg K (2019), Nov. Ingredients for solar-like systems: protostar IRAS 16293-2422 B versus comet 67P/Churyumov-Gerasimenko. *MNRAS* 490 (1): 50–79. doi:10.1093/mnras/stz2430. 1908.11290.

- Du F, Bergin EA, Hogerheijde M, van Dishoeck EF, Blake G, Bruderer S, Cleeves I, Dominik C, Fedele D, Lis DC, Melnick G, Neufeld D, Pearson J and Yıldız U (2017), Jun. Survey of Cold Water Lines in Protoplanetary Disks: Indications of Systematic Volatile Depletion. *ApJ* 842 (2), 98. doi:10.3847/1538-4357/aa70ee. 1705.00799.
- Dullemond CP, Juhasz A, Pohl A, Sereshti F, Shetty R, Peters T, Commercon B and Flock M (2012), Feb. RADMC-3D: A multi-purpose radiative transfer tool, ascl:1202.015.
- Grant SL, van Dishoeck EF, Tabone B, Gasman D, Henning T, Kamp I, Güdel M, Lagage PO, Bettoni G, Perotti G, Christiaens V, Samland M, Arabhavi AM, Argyriou I, Abergel A, Absil O, Barrado D, Boccaletti A, Bouwman J, Caratti o Garatti A, Geers V, Glauser AM, Guadarrama R, Jang H, Kanwar J, Lahuis F, Morales-Calderón M, Mueller M, Nehmé C, Olofsson G, Pantin E, Pawellek N, Ray TP, Rodgers-Lee D, Scheithauer S, Schreiber J, Schwarz K, Temmink M, Vandenbussche B, Vlasblom M, Waters LBFM, Wright G, Colina L, Greve TR, Justannont K and Östlin G (2023), Apr. MINDS. The Detection of $^{13}\text{CO}_2$ with JWST-MIRI Indicates Abundant CO_2 in a Protoplanetary Disk. *ApJL* 947 (1), L6. doi:10.3847/2041-8213/acc44b. 2212.08047.
- Harsono D, Persson MV, Ramos A, Murillo NM, Maud LT, Hogerheijde MR, Bosman AD, Kristensen LE, Jørgensen JK, Bergin EA, Visser R, Mottram JC and van Dishoeck EF (2020), Apr. Missing water in Class I protostellar disks. *A&A* 636, A26. doi:10.1051/0004-6361/201935994. 2002.11897.
- Henning T and Semenov D (2013), Dec. Chemistry in Protoplanetary Disks. *Chemical Reviews* 113 (12): 9016–9042. doi:10.1021/cr400128p. 1310.3151.
- Hily-Blant P, Magalhaes de Souza V, Kastner J and Forveille T (2019), Dec. Multiple nitrogen reservoirs in a protoplanetary disk at the epoch of comet and giant planet formation. *A&A* 632, L12. doi:10.1051/0004-6361/201936750. 1911.06676.
- Hogerheijde MR and van der Tak FFS (2000), Oct. An accelerated Monte Carlo method to solve two-dimensional radiative transfer and molecular excitation. With applications to axisymmetric models of star formation. *A&A* 362: 697–710. doi:10.48550/arXiv.astro-ph/0008169. astro-ph/0008169.
- Ilee JD, Walsh C, Booth AS, Aikawa Y, Andrews SM, Bae J, Bergin EA, Bergner JB, Bosman AD, Cataldi G, Cleeves LI, Czekala I, Guzmán VV, Huang J, Law CJ, Le Gal R, Loomis RA, Ménard F, Nomura H, Öberg KI, Qi C, Schwarz KR, Teague R, Tsukagoshi T, Wilner DJ, Yamato Y and Zhang K (2021), Nov. Molecules with ALMA at Planet-forming Scales (MAPS). IX. Distribution and Properties of the Large Organic Molecules HC_3N , CH_3CN , and $\text{c-C}_3\text{H}_2$. *ApJS* 257 (1), 9. doi:10.3847/1538-4365/ac1441. 2109.06319.
- Kama M, Shorttle O, Jermyn AS, Folsom CP, Furuya K, Bergin EA, Walsh C and Keller L (2019), Nov. Abundant Refractory Sulfur in Protoplanetary Disks. *ApJ* 885 (2), 114. doi:10.3847/1538-4357/ab45f8. 1908.05169.
- Keyte L, Kama M, Chuang KJ, Cleeves LI, Drozdovskaya MN, Furuya K, Rawlings J and Shorttle O (2024), Feb. Spatially resolving the volatile sulfur abundance in the HD 100546 protoplanetary disc. *MNRAS* 528 (1): 388–407. doi:10.1093/mnras/stae019. 2312.13997.
- Law CJ, Loomis RA, Teague R, Öberg KI, Czekala I, Andrews SM, Huang J, Aikawa Y, Alarcón F, Bae J, Bergin EA, Bergner JB, Boehler Y, Booth AS, Bosman AD, Calahan JK, Cataldi G, Cleeves LI, Furuya K, Guzmán VV, Ilee JD, Le Gal R, Liu Y, Long F, Ménard F, Nomura H, Qi C, Schwarz KR, Sierra A, Tsukagoshi T, Yamato Y, van't Hoff MLR, Walsh C, Wilner DJ and Zhang K (2021), Nov. Molecules with ALMA at Planet-forming Scales (MAPS). III. Characteristics of Radial Chemical Substructures. *ApJS* 257 (1), 3. doi:10.3847/1538-4365/ac1434. 2109.06210.
- Le Gal R, Brady MT, Öberg KI, Roueff E and Le Petit F (2019), Dec. The Role of C/O in Nitrile Astrochemistry in PDRs and Planet-forming Disks. *ApJ* 886 (2), 86. doi:10.3847/1538-4357/ab4ad9. 1910.01554.
- Lee JE, Lee S, Baek G, Aikawa Y, Cieza L, Yoon SY, Herczeg G, Johnstone D and Casassus S (2019), Feb. The ice composition in the disk around V883 Ori revealed by its stellar outburst. *Nature Astronomy* 3: 314–319. doi:10.1038/s41550-018-0680-0. 1809.00353.
- Li J, Bergin EA, Blake GA, Ciesla FJ and Hirschmann MM (2021), Apr. Earth's carbon deficit caused by early loss through irreversible sublimation. *Science Advances* 7 (14): eabd3632. doi:10.1126/sciadv.abd3632. 2104.02702.
- Lin ZYD, Li ZY, Tobin J, Jørgensen JK, Looney LW, Aso Y, Takakuwa S, Aikawa Y, van't Hoff MLR, de Gregorio-Monsalvo I, Encalada FJ, Flores C, Gavino S, Han I, Kido M, Koch PM, Kwon W, Lai SP, Lee CW, Lee JE, Phuong NT, Sai JIC, Sharma R, Sheehan P, Thieme TJ, Williams JP, Yamato Y and Yen HW (2023), Jul. Early Planet Formation in Embedded Disks (eDisk). II. Limited Dust Settling and Prominent Snow Surfaces in the Edge-on Class I Disk IRAS 04302+2247. *ApJ* 951 (1), 9. doi:10.3847/1538-4357/acd5c9. 2306.15423.
- Loomis RA, Öberg KI, Andrews SM, Walsh C, Czekala I, Huang J and Rosenfeld KA (2018), Apr. Detecting Weak Spectral Lines in Interferometric Data through Matched Filtering. *AJ* 155 (4), 182. doi:10.3847/1538-3881/aab604. 1803.04987.
- Mah J, Savvidou S and Bitsch B (2024), Jun. Mind the gap: Distinguishing disc substructures and their impact on the inner disc composition. *A&A* 686, L17. doi:10.1051/0004-6361/202450322. 2406.06219.
- Öberg KI, Murray-Clay R and Bergin EA (2011), Dec. The Effects of Snowlines on C/O in Planetary Atmospheres. *ApJL* 743 (1), L16. doi:10.1088/2041-8205/743/1/L16. 1110.5567.
- Öberg KI, Guzmán VV, Walsh C, Aikawa Y, Bergin EA, Law CJ, Loomis RA, Alarcón F, Andrews SM, Bae J, Bergner JB, Boehler Y, Booth AS, Bosman AD, Calahan JK, Cataldi G, Cleeves LI, Czekala I, Furuya K, Huang J, Ilee JD, Kurtovic NT, Le Gal R, Liu Y, Long F, Ménard F, Nomura H, Pérez LM, Qi C, Schwarz KR, Sierra A, Teague R, Tsukagoshi T, Yamato Y, van't Hoff MLR, Waggoner AR, Wilner DJ and Zhang K (2021), Nov. Molecules with ALMA at Planet-forming Scales (MAPS). I. Program Overview and Highlights. *ApJS* 257 (1), 1. doi:10.3847/1538-4365/ac1432. 2109.06268.
- Öberg KI, Facchini S and Anderson DE (2023), Aug. Protoplanetary Disk Chemistry. *ARA&A* 61: 287–328. doi:10.1146/annurev-astro-022823-040820. 2309.05685.
- Paneque-Carreño T, Miotello A, van Dishoeck EF, Tabone B, Izquierdo AF and Facchini S (2023), Jan. Directly tracing the vertical stratification of molecules in protoplanetary disks. *A&A* 669, A126. doi:10.1051/0004-6361/202244428. 2210.01130.
- Pascucci I, Herczeg G, Carr JS and Bruderer S (2013), Dec. The Atomic and Molecular Content of Disks around Very Low-mass Stars and Brown Dwarfs. *ApJ* 779 (2), 178. doi:10.1088/0004-637X/779/2/178. 1311.1228.
- Pinte C, Ménard F, Duchêne G, Hill T, Dent WRF, Woitke P, Maret S, van der Plas G, Hales A, Kamp I, Thi WF, de Gregorio-Monsalvo I, Rab C, Quanz SP, Avenhaus H, Carmona A and Casassus S (2018), Jan. Direct mapping of the temperature and velocity gradients in discs. Imaging the vertical CO snow line around IM Lupi. *A&A* 609, A47. doi:10.1051/0004-6361/201731377. 1710.06450.
- Poch O, Istiqomah I, Quirico E, Beck P, Schmitt B, Theulé P, Faure A, Hily-Blant P, Bonal L, Raponi A, Ciarniello M, Rousseau B, Potin S, Brissaud O, Flandinet L, Filacchione G, Pommerol A, Thomas N, Kappel D, Mennella V, Moroz L, Vinogradoff V, Arnold G, Erard S, Bockelée-Morvan D, Leyrat C, Capaccioni F, De Sanctis MC, Longobardo A, Mancarella F, Palomba E and Tosi F (2020), Mar. Ammonium salts are a reservoir of nitrogen on a cometary nucleus and possibly on some asteroids. *Science* 367 (6483), aaw7462. doi:10.1126/science.aaw7462. 2003.06034.
- Qi C, Öberg KI, Espaillat CC, Robinson CE, Andrews SM, Wilner DJ, Blake GA, Bergin EA and Cleeves LI (2019), Sep. Probing CO and N_2 Snow Surfaces in Protoplanetary Disks with N_2H^+ Emission. *ApJ* 882 (2), 160. doi:10.3847/1538-4357/ab35d3. 1907.10647.
- Rivilla VM, Drozdovskaya MN, Altwegg K, Caselli P, Beltrán MT, Fontani F, van der Tak FFS, Cesaroni R, Vasyunin A, Rubin M, Lique F, Marinakis S, Testi L, Rosina Team, Balsiger H, Berthelier JJ, de Keyser J, Fiethé B, Fuselier SA, Gasc S, Gombosi TI, Sémon T and Tzou CY (2020), Feb. ALMA and ROSINA detections of phosphorus-bearing molecules: the interstellar thread between star-forming regions and comets.

- MNRAS* 492 (1): 1180–1198. doi:10.1093/mnras/stz3336. 1911. 11647.
- Sakai N, Sakai T, Hirota T, Watanabe Y, Ceccarelli C, Kahane C, Bottinelli S, Caux E, Demyk K, Vastel C, Coutens A, Taquet V, Ohashi N, Takakuwa S, Yen HW, Aikawa Y and Yamamoto S (2014), Mar. Change in the chemical composition of infalling gas forming a disk around a protostar. *Nature* 507 (7490): 78–80. doi:10.1038/nature13000.
- Salinas VN, Hogerheijde MR, Mathews GS, Öberg KI, Qi C, Williams JP and Wilner DJ (2017), Oct. DCO⁺, DCN, and N₂D⁺ reveal three different deuteration regimes in the disk around the Herbig Ae star HD 163296. *A&A* 606, A125. doi:10.1051/0004-6361/201731223. 1707. 06475.
- Sturm JA, McClure MK, Beck TL, Harsono D, Bergner JB, Dartois E, Boogert ACA, Chiar JE, Cordiner MA, Drozdovskaya MN, Ioppolo S, Law CJ, Linnartz H, Lis DC, Melnick GJ, McGuire BA, Noble JA, Öberg KI, Palumbo ME, Pendleton YJ, Perotti G, Pontoppidan KM, Qasim D, Rocha WRM, Terada H, Urso RG and van Dishoeck EF (2023), Nov. A JWST inventory of protoplanetary disk ices. The edge-on protoplanetary disk HH 48 NE, seen with the Ice Age ERS program. *A&A* 679, A138. doi:10.1051/0004-6361/202347512. 2309. 07817.
- Tabone B, Bettoni G, van Dishoeck EF, Arabhavi AM, Grant S, Gasman D, Henning T, Kamp I, Güdel M, Lagage PO, Ray T, Vandenbussche B, Abergel A, Absil O, Argyriou I, Barrado D, Boccaletti A, Bouwman J, Caratti o Garatti A, Geers V, Glauser AM, Justannont K, Lahuis F, Mueller M, Nehmé C, Olofsson G, Pantin E, Scheithauer S, Waelkens C, Waters LBFM, Black JH, Christiaens V, Guadarrama R, Morales-Calderón M, Jang H, Kanwar J, Pawellek N, Perotti G, Perrin A, Rodgers-Lee D, Samland M, Schreiber J, Schwarz K, Colina L, Östlin G and Wright G (2023), Jul. A rich hydrocarbon chemistry and high C to O ratio in the inner disk around a very low-mass star. *Nature Astronomy* 7: 805–814. doi:10.1038/s41550-023-01965-3. 2304. 05954.
- Teague R, Bae J, Bergin EA, Birnstiel T and Foreman-Mackey D (2018), Jun. A Kinematical Detection of Two Embedded Jupiter-mass Planets in HD 163296. *ApJL* 860 (1), L12. doi:10.3847/2041-8213/aac6d7. 1805. 10290.
- van der Tak FFS, Black JH, Schöier FL, Jansen DJ and van Dishoeck EF (2007), Jun. A computer program for fast non-LTE analysis of interstellar line spectra. With diagnostic plots to interpret observed line intensity ratios. *A&A* 468 (2): 627–635. doi:10.1051/0004-6361:20066820. 0704. 0155.
- van 't Hoff MLR, Harsono D, Tobin JJ, Bosman AD, van Dishoeck EF, Jørgensen JK, Miotello A, Murillo NM and Walsh C (2020), Oct. Temperature Structures of Embedded Disks: Young Disks in Taurus Are Warm. *ApJ* 901 (2), 166. doi:10.3847/1538-4357/abb1a2.
- Vlasblom M, van Dishoeck EF, Tabone B and Bruderer S (2024), Feb. Mid-infrared spectra of T Tauri disks: Modeling the effects of a small inner cavity on CO₂ and H₂O emission. *A&A* 682, A91. doi:10.1051/0004-6361/202348224. 2311. 12445.
- Walsh C, Loomis RA, Öberg KI, Kama M, van 't Hoff MLR, Millar TJ, Aikawa Y, Herbst E, Wicidius Weaver SL and Nomura H (2016), May. First Detection of Gas-phase Methanol in a Protoplanetary Disk. *ApJL* 823 (1), L10. doi:10.3847/2041-8205/823/1/L10. 1606. 06492.
- Wilson TL and Rood R (1994), Jan. Abundances in the Interstellar Medium. *ARA&A* 32: 191–226. doi:10.1146/annurev.aa.32.090194.001203.
- Yen HW, Koch PM, Liu HB, Puspitaningrum E, Hirano N, Lee CF and Takakuwa S (2016), Dec. Stacking Spectra in Protoplanetary Disks: Detecting Intensity Profiles from Hidden Molecular Lines in HD 163296. *ApJ* 832 (2), 204. doi:10.3847/0004-637X/832/2/204. 1610. 01780.
- Yoshida TC, Nomura H, Furuya K, Tsukagoshi T and Lee S (2022), Jun. A New Method for Direct Measurement of Isotopologue Ratios in Protoplanetary Disks: A Case Study of the ¹²CO/¹³CO Ratio in the TW Hya Disk. *ApJ* 932 (2), 126. doi:10.3847/1538-4357/ac6efb. 2204. 08330.
- Zhang K (2024), Jul. Chemistry in Protoplanetary Disks. *Reviews in Mineralogy and Geochemistry* 90 (1): 27–53. doi:10.2138/rmg.2024.90.02. 2404. 15423.